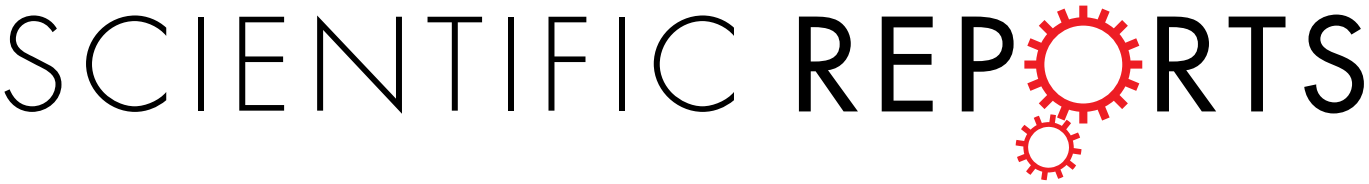

OPEN

# Carbon and Nitrogen Speciation in N-poor C-O-H-N Fluids at 6.3 GPa and 1100–1400 °C

Received: 9 January 2017
Accepted: 8 March 2017
Published online: 06 April 2017

Alexander G. Sokol[1,2], Anatoly A. Tomilenko[1], Taras A. Bul'bak[1], Galina A. Palyanova[1,2], Ivan A. Sokol[1] & Yury N. Palyanov[1,2]

**Deep carbon and nitrogen cycles played a critical role in the evolution of the Earth. Here we report on successful studying of speciation in C-O-H-N systems with low nitrogen contents at 6.3 GPa and 1100 to 1400 °C. At $fO_2$ near Fe–FeO (IW) equilibrium, the synthesised fluids contain more than thirty species. Among them, $CH_4$, $C_2H_6$, $C_3H_8$ and $C_4H_{10}$ are main carbon species. All carbon species, except for $C_1$-$C_4$ alkanes and alcohols, occur in negligible amounts in the fluids generated in systems with low $H_2O$, but $C_{15}$-$C_{18}$ alkanes are slightly higher and oxygenated hydrocarbons are more diverse at higher temperatures and $H_2O$ concentrations. At a higher oxygen fugacity of +2.5 $\Delta\log fO_2$ (IW), the fluids almost lack methane and contain about 1 rel.% $C_2$-$C_4$ alkanes, as well as fractions of percent of $C_{15–18}$ alkanes and notable contents of alcohols and carboxylic acids. Methanimine ($CH_3N$) is inferred to be the main nitrogen species in N-poor reduced fluids. Therefore, the behaviour of $CH_3N$ may control the nitrogen cycle in N-poor peridotitic mantle. Oxidation of fluids strongly reduces the concentration of $CH_4$ and bulk carbon. However, higher alkanes, alcohols, and carboxylic acids can resist oxidation and should remain stable in mantle hydrous magmas.**

Abiotic hydrocarbons (HCs) and ammonia have been important agents in the Earth's carbon and nitrogen cycles. Their stability in different tectonic settings in the course of geodynamic evolution could control the habitability of the planet, the amounts of carbon and nitrogen migrating in fluids, the processes of redox melting and freezing, and the formation of diamonds[1–6]. There is a wealth of evidence for the existence of hydrocarbons in the mantle. Namely, Sugisaki and Mimura (ref. 7) studied a collection of 227 samples from fifty localities throughout the world and revealed heavy hydrocarbons (n-alkanes) in mantle-derived rocks, such as peridotites in ophiolite sequences or peridotite xenoliths in alkali basalts, but did not find any in gabbro and granite. HCs in inclusions hosted by diamond and other minerals in mantle xenoliths were reported from the Siberian craton[8–11]. As a recent find, we can cite a thin fluid jacket of $CH_4$ around inclusions of solidified iron-nickel-carbon-sulfur melt in large, exceptional gem (like the Cullinan, Constellation, and Koh-i-Noor) sublithospheric diamonds reported by Smith *et al.* (ref. 12).

The genesis of hydrocarbons in the mantle remains unclear. They might be a mixture of HCs which were recycled or delivered by meteorites and comets to the early (primeval) Earth, or synthesised by the Fischer-Tropsch reaction[7]. The contribution of two former sources may be, however, limited: HCs may oxidise during subduction and can hardly survive the high impact temperatures. The composition of hydrocarbons may vary. For instance, HCs heavier than methane were inferred[13–17] to be energetically favoured at the deep mantle *P-T* conditions. As for nitrogen in reduced mantle, there is a consensus that most of it resides in ammonia and $NH_4^+$ which substitutes for alkali cations in phengite, Cr-bearing clinopyroxene and other silicates[2,18,19].

The behaviour of carbon and nitrogen species in mantle fluids depends on oxygen fugacity ($fO_2$). Estimates for continental lithospheric mantle (CLM) within the Kaapvaal[20], Slave[21] and Siberian[22,23] cratons show that $fO_2$ generally decreases depthward from +1 $\Delta\log fO_2$ FMQ (Fayalite-Magnetite-Quartz oxygen buffer) at 100 km (~3.2 GPa) to −4 $\Delta\log fO_2$ FMQ at a depth of 220 km (~7 GPa). The $fO_2$ values at the CLM base about 200 km below the surface may vary from IW + 1 to IW + 3 log units[1] and the temperatures at this depth may range within 1100–1400 °C[20–23]. According to thermodynamic calculations, lower alkanes (especially methane and ethane) and ammonia are expected to be stable under $fO_2$ conditions of the CLM[3,24–26], but they almost disappear from

[1]V.S. Sobolev Institute of Geology and Mineralogy, Siberian Branch of the Russian Academy of Sciences, ave. Koptyuga 3, Novosibirsk, 630090, Russia. [2]Novosibirsk State University, str. Pirogova 2, Novosibirsk, 630090, Russia. Correspondence and requests for materials should be addressed to A.G.S. (email: sokola@igm.nsc.ru)

| Run# | Graphite | Docosane ($C_{22}H_{46}$) | Stearic acid ($C_{18}H_{36}O_2$) |
|---|---|---|---|
| 1761_2_3 | 18.7 | 1.8 | — |
| 1769_2_2 | 8 | 0.3 | 0.3 |
| 1315_3_5 | 26.2 | — | 3.1 |
| 1751_2_2 | 8.8 | — | 0.9 |
| 1751_2_3 | 9 | 0.6 | — |
| 1746_2_3 | 9.4 | 0.7 | — |
| 1746_2_2 | 8.4 | — | 0.9 |
| 1780_2_2 | 7.6 | — | 0.7 |
| 1780_2_3 | 8.1 | 0.8 | — |
| 1780_2_4 | 8.3 | — | 1.0 |
| 1016_7_2 | 8.2 | — | 0.5 |
| 1016_7_4 | 8.8 | 0.6 | — |
| 1753_2_3 | 18.6 | — | 1.7 |
| 1898_2_1 | 7.1 | — | 0.5 |
| 1898_2_3 | 7.8 | 0.3 | 0.3 |
| 888_7_1 | 23 | 1.9 | — |
| 889_7_1 | 23.7 | 1.4 | — |
| 1720_2_2 | 17.7 | — | 3.2 |
| 1727_2_2 | 17.8 | 3.9 | — |
| 1019_7_1 | 8.1 | — | 0.7 |
| 1019_7_3 | 7.3 | 0.4 | 0.3 |

**Table 1.** Starting compositions (mg). Microscopic amounts of nitrogen in the capsules came from air.

fluids at $fO_2$ reaching CW (the maximum $H_2O$ content in C-O-H fluids). Moreover, the silicate environment can influence the pH of deep $H_2O$-bearing fluids and thus the carbon and nitrogen speciation[6,26,27].

Recent decades have brought much progress in experimental techniques with $fO_2$ and $fH_2$ buffering used to predict potential compositions of hydrocarbon fluids at mantle pressures and temperatures. Carbon-saturated C-O-H fluids in reduced systems were studied by quenching experiments and chromatography at 2.0–3.5 GPa and 1000–1300 °C[28,29], as well as at 5.7–6.3 GPa and 1200–1600 °C[30,31]. Carbon concentrations in strongly reduced fluids synthesised under these $P$-$T$-$fO_2$ conditions are commonly related as $CH_4 > C_2H_6 > C_3H_8$ (other HCs being ≪1%) and agree well with calculations[20,25,28,32]. The concentrations of lower alkanes at pressures from 4 to 7 GPa and typical CLM temperatures[25,32,33] vary only little, but the precise contents of other hydrocarbons remain unknown. Among nitrogen species, ammonia was reported[3] to predominate in nitrogen rich N-O-H fluids entrapped in quartz and olivine at 0.2–3.5 GPa, 600–1400 °C and $fO_2$ at the Fe-FeO equilibrium, as well as in ultra-reduced nitrogen-rich C-O-H-N fluids at 5.5–7.8 GPa and 1100–1500 °C, as shown by our recent experiments[34]. In upper mantle aqueous fluids under reducing conditions, nitrogen is expected to occur mainly as ammonium ($NH_4^+$)[26].

In this study we apply quenching experiments with buffered hydrogen fugacity to study (i) the stability of different carbon and nitrogen species in N-poor C-O-H-N fluids at 6.3 GPa, 1100–1400 °C and $fO_2$ about or slightly below IW corresponding to the conditions at the CLM base (~200 km depth) near the boundary with the asthenosphere, and (ii) the relative stability of HCs and N-bearing compounds at $fO_2$ IW +2.5 log units corresponding to reactions of reduced C-O-H-N fluids with oxidised lithosphere. The estimates[25,32,33] that the fluid composition does not depend much on pressure within 4–7 GPa allows us to extrapolate the results onto the upper mantle pressure range.

## Results

**Effect of cooling rate on behaviour of C-O-H-N fluids.** Isobaric cooling can change the compositions of fluids as a result of back reactions. In this respect, it is critical for the fluids to cool down at rates sufficient for precluding back reactions and holding the equilibrium composition consistent with the target temperature and run duration. Changes in the species composition of fluids were studied previously in 2.4 GPa experiments in the C-O-H system synthesised at 1000 °C and cooling at rates from 0.3 to 120 deg/s at buffered $fO_2$[29]. The potential effect was monitored against concentration changes of species involved in the $C_2H_6 + H_2 \rightarrow 2CH_4$ reaction, and back reactions were shown to stop completely only at relatively rapid cooling of 120 deg/s. The fluids cooling at slower rates contained less hydrogen (2 to 4 mol.%) and, correspondingly, more $CH_4$. The closure temperature for the C-O-H system equilibration was suggested to be <800 °C[29]. Earlier we[31] investigated the effect of cooling rates in the range of 1 to 200 deg/s on the composition of C-O-H fluids synthesised at 6.3 GPa and 1600 °C in 15 hr-long runs. Comparison of fluids generated from the same starting materials but cooled at different rates showed $CH_4$ and $C_2H_6$ to increase from 2–3 to 9–10 mole % and from 1 to 3 mole %, respectively, as cooling slowed down from 200 to 27 deg/s. Further deceleration to 1 deg/s did not change the concentration of $CH_4$, but led to $C_2H_6$ increase from 3 to 4–5 mol.%. Therefore, synthesis of hydrocarbons most likely was due to back reactions of hydrogen with graphite during slow cooling, as we suggested[31]. Meanwhile, the changes of nitrogen speciation in O-H-N

| Run# | Starting composition* | Capsule | Buffer $fH_2$ | Time (h) | T (°C) | $H_2O$ | $CH_4$ | $C_2H_6$ | $C_3H_8$ | $C_4H_{10}$ | $CH_3N/(CH_3N+N_2)$ | Calc. $fO_2$ |
|---|---|---|---|---|---|---|---|---|---|---|---|---|
| 1761_2_3 | Docosane | Pt | MMO | 0.017 | 1100 | 11 | 10 | 74 | 5.2 | 0.2 | 1.00 | — |
| 1769_2_2 | Stearic acid + docosane | Pt | MMO | 7 | 1100 | 16 | 35 | 31 | 14 | 0.2 | 0.22 | −10.8 |
| 1315_3_5 | Stearic acid | Pt | — | 7 | 1200 | 93 | 2.9 | 0.7 | 0.4 | 1.0 | 0.03 | −8.5 |
| 1751_2_2 | Stearic acid | Au | MMO | 7 | 1200 | 41 | 37 | 18 | 2.7 | 0.2 | 0.99 | −10.8 |
| 1751_2_3 | Docosane | Au | MMO | 7 | 1200 | 9.6 | 50 | 31 | 8.1 | 0.4 | 0.99 | −15.4 |
| 1746_2_3 | Docosane | Pt | MMO | 2 | 1300 | 11 | 26 | 38 | 21 | 1.7 | 0.80 | −9.0 |
| 1746_2_2 | Stearic acid | Pt | MMO | 2 | 1300 | 39 | 23 | 28 | 5.0 | 1.8 | 0.98 | −10.5 |
| 1780_2_2 | Docosane | Pt | MMO | 7 | 1300 | 4.2 | 27 | 36 | 24 | 5.7 | 0.95 | −9.3 |
| 1780_2_3 | Stearic acid | Pt | MMO | 7 | 1300 | 55 | 13 | 24 | 4.9 | 0.9 | Only $N_2$ | −8.5 |
| 1780_2_4 | Stearic acid*** | Pt | MMO | 7 | 1300 | 6.9 | 5.2 | 4.2 | 0.2 | 0.02 | Only $N_2$ | — |
| 1016_7_2 | Stearic acid | Pt | MMO | 0.017 | 1400 | 25 | 11 | 31 | 23 | 3.6 | 0.93 | — |
| 1016_7_4 | Docosane | Pt | MMO | 0.017 | 1400 | 32 | 11 | 31 | 17 | 4.2 | 0.93**** | — |
| 1753_2_3 | Stearic acid | Pt | MMO | 2 | 1400 | 31 | 38 | 20 | 8.6 | 2.2 | Only $CH_3N$ | −10.6 |
| 1898_2_1 | Stearic acid | Pt | MMO | 2 | 1400** | 30 | 16 | 32 | 15 | 2.2 | 1.00 | −10.5 |
| 1898_2_3 | Stearic acid + docosane | Pt | MMO | 2 | 1400** | 24 | 17 | 35 | 14 | 2.2 | 1.00 | −10.9 |
| 888_7_1 | Docosane | Pt | MMO | 2 | 1400** | 4.4 | 23 | 71 | 0.8 | 1.0 | 1.00 | — |
| 889_7_1 | Docosane | Pt | MMO | 7 | 1400 | 0.7 | 51 | 38 | 8.7 | 0.6 | 0.69 | — |
| 1720_2_2 | Stearic acid | Pt | — | 7 | 1400 | 96 | 0.06 | 1.4 | 0.08 | 0.8 | Only $N_2$ | −6.0 |
| 1727_2_2 | Docosane | Pt | MMO | 7 | 1400 | 11 | 22 | 34 | 4.9 | 3.5 | 0.72 | −8.8 |
| 1019_7_1 | Stearic acid | Pt | MMO | 10 | 1400 | 52 | 18 | 25 | 2.7 | 1.5 | 0.98 | −8.1 |
| 1019_7_3 | Stearic acid + docosane | Pt | MMO | 10 | 1400 | 26 | 18 | 35 | 14 | 3.3 | 0.99 | −11.0 |

**Table 2.** Experimental conditions and concentrations of main species (rel.%) in quenched C-O-H-N fluids synthesised at 6.3 GPa. Full compositions are given in Supplementary Table 1. MMO is Mo-$MoO_2$ buffer. $CH_3N/(CH_3N+N_2)$ is normalised peak area ratio $A(17+29\,m/z)/(A(17+29\,m/z)+A(28\,m/z))$. *All starting compositions include graphite, at 10/1 to fluid generating material. **Fluid cooling at 1 deg/s. ***Very little gas released upon capsule opening. ****$NH_3$ is main nitrogen species.

fluids at cooling rates from 70 to 140 deg/s in the forward and reversal experiments of Li and Keppler (ref. 3) were negligible, if any.

In this study we have performed three 2-hr long runs at 1400 °C, with quenching at 200 deg/s and slow cooling at 1 deg/s (Tables 1–3). The normalised peak areas for particular species in GC-MS spectra showed slight variations in lower alkanes in slowly cooling fluids with similar amounts of water (24–31 rel.%). The $CH_4/C_2H_6$ ratio was above and below 1 at rapid and slow cooling, respectively. Cooling at 200 times slower rates did not cause notable changes to $CH_4$, $C_2H_6$, $C_3H_8$ and $C_4H_{10}$ concentrations (Table 2) but led to about ten-fold increase of $C_{15}$ to $C_{19}$ alkanes (from ~0.01 to ~0.1) and formation of minor amounts (within ~0.5 rel.%) of olefins, arenes, and oxygenated hydrocarbons: aldehydes, ketones, and carboxylic acids (specifically, 0.2 rel.% acetic acid and higher concentrations of acids with $C_{10}$, $C_{13}$ and $C_{15}$). Note especially that slow cooling resulted in the formation of more methanimine ($CH_3N$), at the same $P$-$T$-$\tau$ conditions as during quenching (Table 2).

Therefore, back reactions in slowly cooling C-O-H-N fluids have different directions at the pressures 2.4 GPa and 6.3 GPa. Cooling leads mainly to synthesis of $CH_4$ and consumption of alkanes by the reaction $C_2H_6 + H_2 = 2CH_4$ at the lower pressure[29], but $CH_4$ either increases[31] or decreases (this study) slightly at 6.3 GPa, while the ratios of $CH_4$ to $C_2H_6$, $C_3H_8$ and $C_4H_{10}$ at high and low cooling rates scatter within a reasonable error. However, slow cooling fluids obtained in this study are remarkable by higher concentrations of species that trace the back reactions (some olefins, arenes, aldehydes, ketones, and carboxylic acids). Thus, our and published data, including our previous results for 6.3 GPa and 1600 °C[31], indicate that only cooling from 1100–1400 °C to room temperature at a rate of 200 deg/s can be interpreted as quenching. Note that only quenching can provide reliable molecular compositions of fluids at the $P$–$T$ conditions of the experiments.

**Kinetics of C-O-H-N fluid equilibration.** The effect of kinetics on concentrations of species that form in the C-O-H-N system at 6.3 GPa and 1400 °C was studied in quenching experiments of different durations from 1 min to 10 hours (Fig. 1 and Table 2). The diversity of alkanes revealed by the GC-MS analysis after capsule opening showed almost no run duration dependence. Lower alkanes, which are the dominant carbon species in the C-O-H-N fluids at 1400 °C, did not change much the $CH_4/C_2H_6$, $CH_4/C_3H_8$ and $CH_4/C_4H_{10}$ ratios of normalised peak areas at longer durations, irrespective of the starting charge composition (Fig. 2). They were slightly higher in fluids generated in longer runs from samples with docosane or stearic acid and remained almost the same in the case of the docosane + stearic acid mixture: the $CH_4/C_2H_6$ ratio was about 1 in all cases and $CH_4/C_3H_8$ varied from 1 to 10. Note that $CH_4/C_4H_{10}$ reached or slightly exceeded 100 in fluids obtained in 2- and 7-hr long runs from samples with docosane at low $H_2O$ concentrations but remained below 10 in the case of relatively high $H_2O$ concentrations with docosane + stearic acid mixture and stearic acid as starting materials.

| Run# | | 1753_2_3 | 1898_2_3 | 1898_2_1 |
|---|---|---|---|---|
| Capsule | | Pt | Pt | Pt |
| Starting composition* | | Stearic acid | Stearic acid + docosane | Stearic acid |
| Cooling rate | | 200 deg/s | 1 deg/s | 1 deg/s |
| Water | | 30.8 | 24.3 | 29.7 |
| Alkanes | $CH_4$ | 37.6 | 17.0 | 16.1 |
| | $C_2H_6$ | 20.0 | 34.5 | 31.9 |
| | $C_3H_8$ | 8.6 | 14.3 | 14.9 |
| | $C_4H_{10}$ | 2.2 | 2.1 | 2.2 |
| | $C_5H_{12}$ | 0.08 | 0.1 | 0.09 |
| | $C_6$-$C_{15}$ | ≤0.002 | ≤0.04 | ≤0.03 |
| | $C_{15}$-$C_{19}$** | ≤0.01 | ≤0.3 | ≤0.1 |
| Olefins | | — | ≤0.06 | ≤0.02 |
| Arenes | | — | ≤0.008 | ≤0.02 |
| Alcohols and ethers | | ≤0.1 | ≤0.1 | ≤0.08 |
| Aldehydes | | — | ≤0.07 | ≤0.08 |
| Ketones | | ≤0.005 | ≤0.03 | ≤0.05 |
| Carboxylic acid | | — | ≤0.5 | ≤0.05 |
| Furans | | ≤0.001 | ≤0.01 | ≤0.03 |
| Nitrogen species | | | | |
| $N_2$ | | — | 0.05 | 0.01 |
| $CH_3N$ | | 0.5 | >1 | >1 |

**Table 3.** Representative analyses of quenched and slow cooling C-O-H-N fluids (rel.%) obtained in 2-hr runs at 6.3 GPa and 1400 °C. *All samples contained graphite. **The quoted concentrations are maximum for a species of the respective group. All GC-MS data are given in Supplementary Table 1.

Olefins, arenes, alcohols, aldehydes, ketones, and carboxylic acids, as well as N-bearing spices, were more diverse in the shortest 1-min runs. Note that the species diversity of oxygenated hydrocarbons was notably smaller in 2-hr experiments but greater in the longest runs (10 hr), though remained below the level of the 1-min run (Fig. 1; 2-hr runs at slow cooling (white histograms) are shown for comparison). Thus the quenched non-equilibrium C-O-H-N fluids obtained in short runs had strongly variable concentrations and high diversity of olefins, arenes, alcohols and ethers, aldehydes, ketones and carboxylic acids, as well as nitrogen-bearing species. The behaviour of these components can be used as evidence of a non-equilibrium composition of reduced fluids.

At 1100 °C, the concentrations of main alkanes and the diversity of oxygenated hydrocarbons in C-O-H-N fluids differed notably in the shortest (1-min) and 7-hour long runs (Tables 2–4). Note that methane was very low while ethane was high ($CH_4/C_2H_6 = 0.14$) in the shortest run, but their concentrations became similar ($CH_4/C_2H_6 = 1.14$) and commensurate with those at 1400 °C at the 7 hr duration. The quenched fluids obtained in 7-hr runs at 1100 °C almost lacked oxygenated hydrocarbons, except for some alcohols and ethers and furans. This data shows that the C-O-H-N fluids resulting from thermal decomposition of higher alkanes at 6.3 GPa and 1400 °C can attain equilibrium already in 2-hr runs, while the attainment of equilibrium at 1100 °C most likely requires at least 7-hr durations. Interestingly, alkanes reached equilibrium concentrations in 1 min at 1400 °C, while fluids synthesised in 1-min long runs at 1100 °C were very rich in ethane.

**Speciation of fluids at $fO_2$ near IW.** We have compared the compositions of carbon and nitrogen species in equilibrated C-O-H-N fluids generated by thermal destruction of docosane in 7-hr long runs at 1100–1200 °C and in ≥ 2-hr runs at 1300–1400 °C (Tables 2 and 4; Figs 3 and 4a), at $H_2O$ from <1 to 11.2 rel.% ($CO_2$ within 0.006 rel.%; CO not detected). Note that the chosen $fH_2$ buffering technique provided $Fe^{3+}$ to $Fe^0$ reduction in a 10-hr test run (Supplementary materials, Figs 1–3). At a higher temperature of 1400 °C, the number of detected alkanes increased from 7–11 at 1200–1300 °C to 14 and even reached 29 in one run. The methane-to-ethane ratios (normalised peak areas) varied from slightly above to slightly below 1, while the $CH_4/C_3H_8$ and $CH_4/C_4H_{10}$ ratios were 1 to 30 and ~100, respectively, without any distinct trend (Fig. 4a). Other species were found in minor amounts of <1 rel.%, except for 0.2 rel.% $C_{16}$-$C_{17}$ alkanes and 0.4 rel.% $C_{18}$ in one run at 1300 °C (Table 4, Supplementary Table 1) against ≤0.01 rel.% in all other runs. Aldehydes and ketones likewise were more diverse in higher-temperature runs at 1400 °C (Fig. 3; white histograms are species in Au capsules), while the number of alcohols and ethers remained approximately the same.

As for nitrogen speciation, the experimental results (Tables 2, 4, Supplementary Table 1) showed methanimine ($CH_3N$, CAS # 2053-29-4) to be the predominant nitrogen host in N-poor C-O-H-N fluids. However, $N_2$ was persistent, though minor (0.1 to 0.01 rel.%), even in ultra-reduced C-O-H-N fluids resulting from decomposition of docosane, with the $CH_3N/N_2 > 2$ ratio in all cases. Ammonia appeared in a single 1-min run at 1400 °C, with its concentration notably exceeding both $N_2$ and $CH_3N$. Other nitrogen species were detectable in trace amounts (Fig. 3 and Supplementary Table 1).

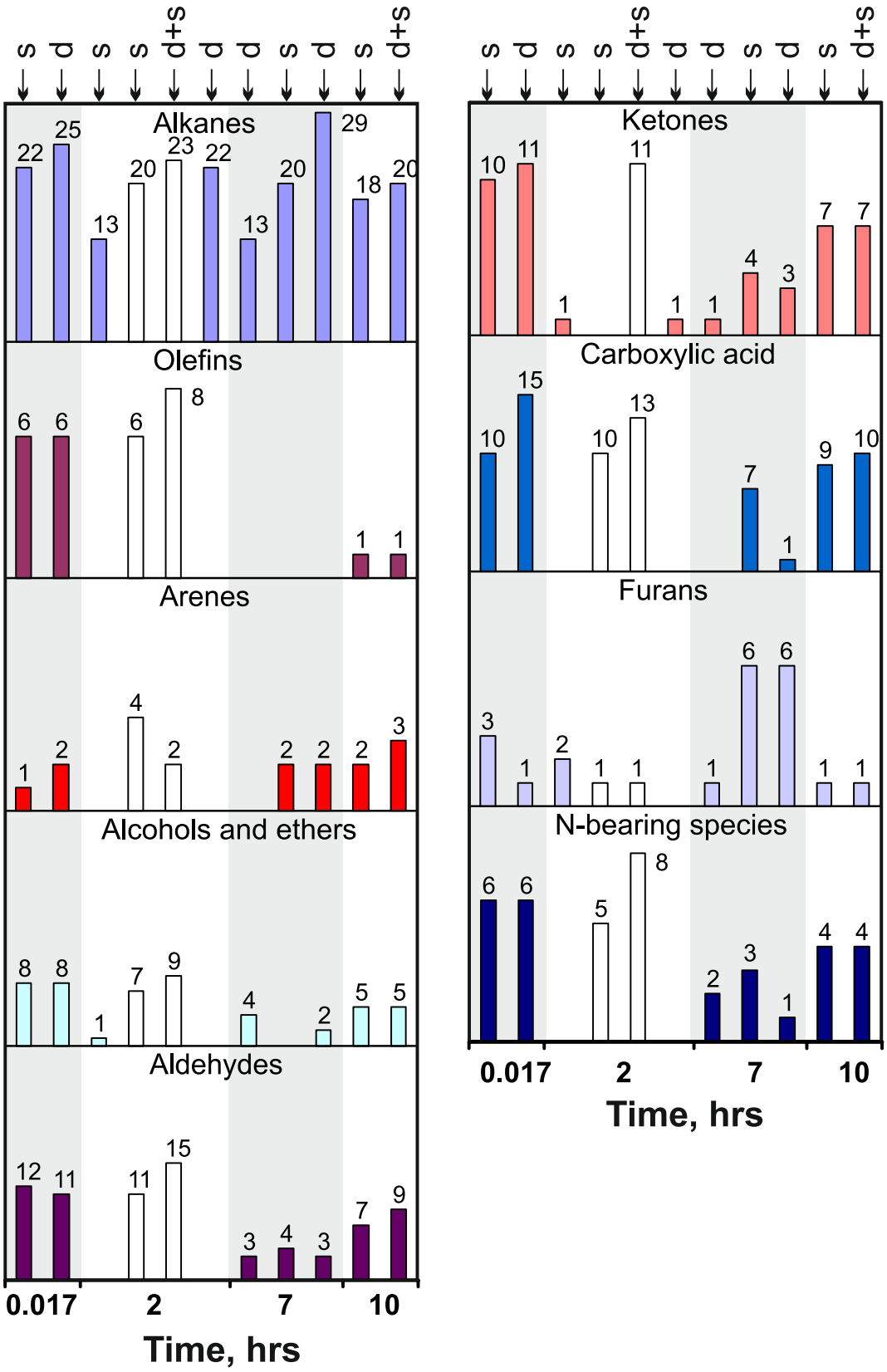


**Figure 1.** Diversity of alkanes, alkenes, and oxygenated hydrocarbons revealed by GC-MS analysis in quenched C-O-H-N fluids at 6.3 GPa, 1400 °C, MMO-buffered $fH_2$ and run durations from 0.017 to 10 hours. Symbols on top show starting compositions of charges for fluid generation: d = docosane; d + s = docosane + stearic acid mixture; s = stearic acid. White columns are unquenched samples cooled down at 1 deg/s. Grey and white bands show run groups.

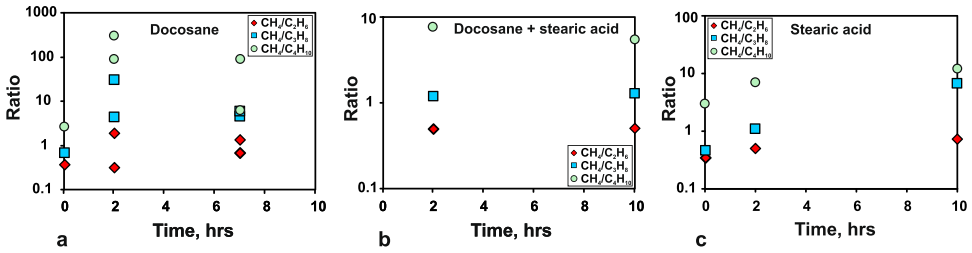


**Figure 2.** Normalised peak area ratios of $CH_4/C_2H_6$, $CH_4/C_3H_8$ and $CH_4/C_4H_{10}$ as a function of duration, according to GC-MS analysis of quenched fluids synthesised at 6.3 GPa and 1400 °C from different starting compositions: a = docosane; b = docosane + stearic acid mixture; c = stearic acid.

| Run# | | 1761_2_3** | 1751_2_3 | 1780_2_2 | 1727_2_2 | 889_7_1 |
|---|---|---|---|---|---|---|
| Capsule | | Pt | Au | Pt | Pt | Pt |
| Temperature (°C) | | 1100 | 1200 | 1300 | 1400 | 1400 |
| Duration (hr) | | 0.017 | 7 | 7 | 7 | 7 |
| Starting composition: Docosane* | | | | | | |
| Water | | 10.4 | 9.5 | 4.2 | 11 | 0.7 |
| Alkanes | $CH_4$ | 10.0 | 49.7 | 26.9 | 22.3 | 51.0 |
| | $C_2H_6$ | 73.8 | 31.1 | 36.5 | 33.9 | 38.5 |
| | $C_3H_8$ | 5.2 | 8.1 | 23.9 | 4.9 | 8.7 |
| | $C_4H_{10}$ | 0.2 | 1.1 | 5.7 | 3.5 | 0.6 |
| | $C_5H_{12}$ | 0.01 | 0.05 | 0.2 | 1.5 | 0.001 |
| | $C_6$-$C_{15}$ | ≤0.002 | — | — | ≤0.6 | ≤0.01 |
| | $C_{15}$-$C_{19}$*** | ≤0.004 | — | ≤0.4 | ≤0.2 | ≤0.01 |
| Olefins | | ≤0.001 | — | | — | — |
| Arenes | | ≤0.001 | — | — | ≤0.6 | — |
| Alcohols and ethers | | ≤0.006 | ≤0.05 | ≤0.1 | ≤0.06 | ≤0.2 |
| Aldehydes | | — | — | — | ≤0.3 | ≤0.001 |
| Ketones | | — | — | — | ≤0.6 | ≤0.002 |
| Carboxylic acid | | ≤0.002 | — | — | ≤0.2 | — |
| Furans | | ≤0.001 | — | — | — | — |
| Nitrogen species | | | | | | |
| $N_2$ | | 0.01 | 0.02 | 0.1 | 0.3 | 0.02 |
| $CH_3N$ | | >1 | >1 | >1 | 0.7 | 0.05 |

**Table 4.** Representative analyses of quenched reduced C-O-H-N fluids (rel.%) obtained in runs at 6.3 GPa and 1100–1400 °C. *All samples contained graphite; **Data given for comparison. ***The quoted concentrations are maximum for a species of the respective group. All GC-MS data are given in Supplementary Table 1.

**Speciation of fluids at $fO_2$ slightly above IW.** The normalised peak areas of water in the chromatograms of quenched equilibrium fluids generated by thermal decomposition of stearic acid or the stearic acid + docosane mixture varied from 16 to 55 rel.%. The concentration of $CO_2$ reached 0.9 rel.% at 1100 °C but decreased to 0.01–0.1 rel.% at 1300–1400 °C. No CO was detectable at higher water contents, as in the case of more reduced fluids. $C_1$-$C_4$ alkanes in C-O-H-N fluids showed more prominent trends with increasing water contents (Figs 2–5). As the run temperature increased to 1400 °C instead of 1200 °C, the $CH_4/C_2H_6$ ratio of normalised peak areas decreased only from slightly above 1 to slightly below 1, as at low $H_2O$, but the $CH_4/C_3H_8$ and $CH_4/C_4H_{10}$ ratios became ten times smaller: from 10 to 1 and from 100 to 10, respectively. Note that $CH_4/C_4H_{10}$ at 1400 °C were much lower at high than at low water contents.

Synthesis in Pt capsules at 1100 and 1300 °C gave fluids with $C_{16}$-$C_{19}$ alkanes from 0.2 to 0.9 rel.% and to 0.2 rel.%, respectively (Table 5). The respective alkane contents in fluids from Au capsules at 1200 °C were no higher than 0.06 rel.% and were still lower in Pt capsules at 1400 °C. Oxygenated hydrocarbons in the fluids were diverse in both Au and Pt capsules (Fig. 3). The contents of the detected species did not show marked variation trends. Among oxygenated hydrocarbons, alcohols and carboxylic acids had the largest contents. Note that a water-rich quenched fluid synthesised at 1300 °C in a 7-hr long run contained 0.1 rel.% methanol, ethanol, and benzoic acid ($C_7H_6O_2$).

Methanimine ($CH_3N$) was the main nitrogen species of C-O-H-N fluids at high-$H_2O$ as well (Table 2, Fig. 6 and Supplementary Table 1), but no ammonia was detected in any run. Persistent $N_2$, from 0.02 to 0.4 rel.%, was observed in the fluids generated by decomposition of stearic acid or the stearic acid + docosane mixture, as in the case of reduced fluids. The normalised peak area ratios corresponding to $CH_3N/N_2$ in quenched fluids were

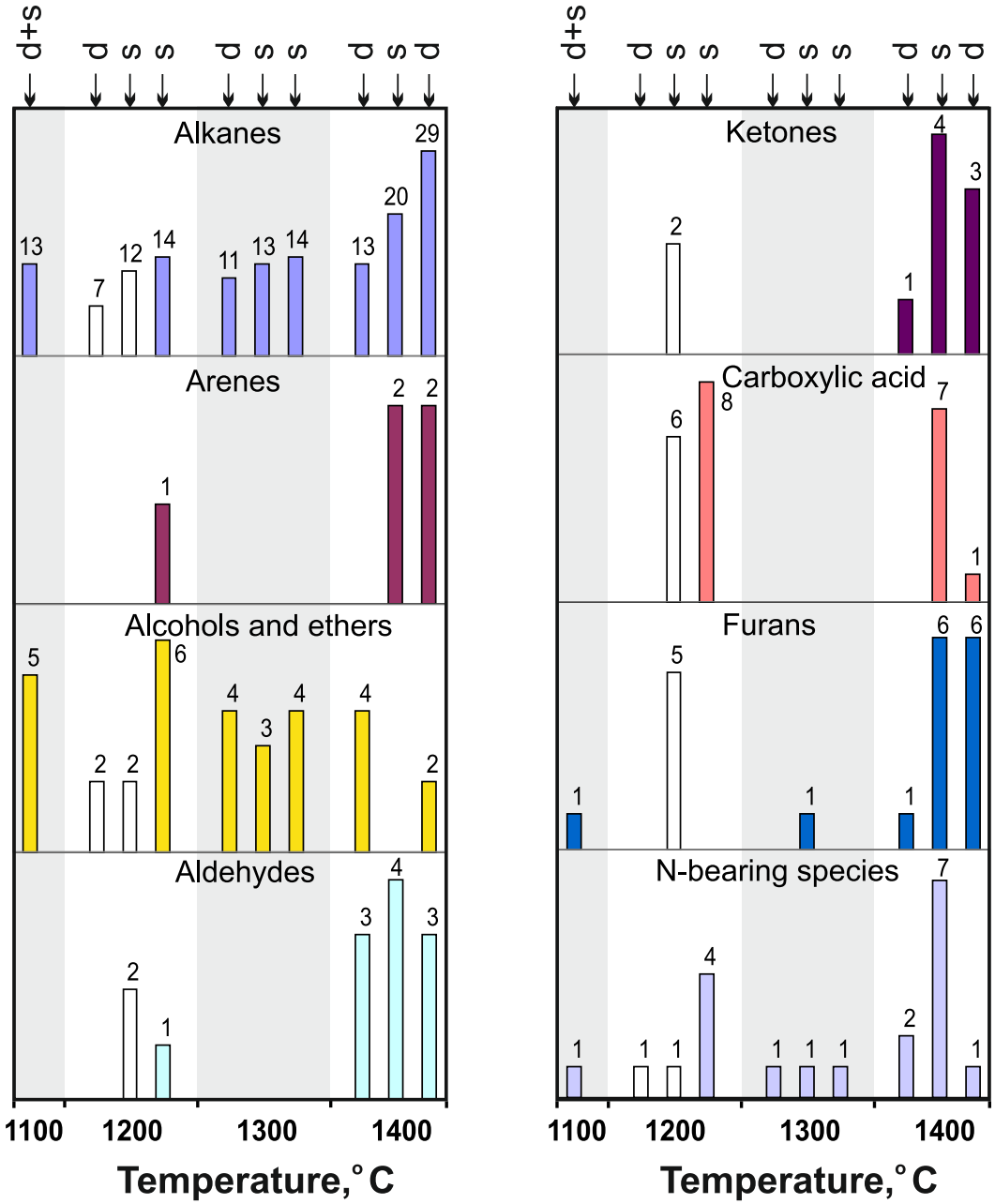


**Figure 3.** Diversity of alkanes, alkenes, and oxygenated hydrocarbons revealed by GC-MS analysis in quenched C-O-H-N fluids at 6.3 GPa, 1100–1400 °C, MMO-buffered $fH_2$ and run durations ≥ 2 hours. White columns are samples obtained in Au capsules. Letter symbols are same as in Fig. 2.

A(17 + 29 m/z)/A(28 m/z) ≫ 1 in most of analysed spectra. Methanimine predominated in the fluids from both Au and Pt capsules. It was found in small amounts only in four runs with Pt capsules (out of those, $fH_2$ was not buffered in two runs and little fluid was released upon capsule opening in one run). Note that the concentration of $CH_3N$ increased at slow cooling (Fig. 6a,b).

**Composition of fluids near CW.** Oxygen fugacity of C-O-H-N fluids could reach the water maximum (CW) in two unbuffered runs at 1200 and 1400 °C (Table 6) because of hydrogen leakage[30,31]. The loss of hydrogen from the fluid led to its water enrichment and oxidation of the hydrocarbons originally produced by thermal decomposition of the starting materials. Contrary to our expectations, HCs demonstrated different degrees of stability to oxidation. The concentrations of methane and ethane decreased dramatically from 20–30% to a few percent and even to fractions of percent (Table 6) while the $C_3$, $C_4$ and $C_5$ alkanes remained almost invariable. Some higher alkanes, especially, $C_{16}$, were present in notable amounts: 0.04 rel.% at 1200 °C to 0.2 rel.% at 1400 °C. In the lower-temperature runs phtalates were observed as the main species among oxygenated hydrocarbons, possibly as a result of capsule contamination. The detected species were markedly more diverse in higher-temperature

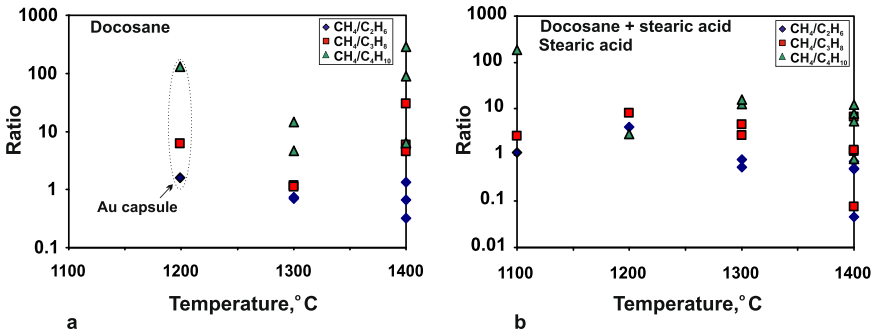


**Figure 4.** Normalised peak area ratios of $CH_4/C_2H_6$, $CH_4/C_3H_8$ and $CH_4/C_4H_{10}$ as a function of temperature, according to GC-MS analysis of quenched fluids synthesised at 6.3 GPa from different starting compositions: a = docosane; b = docosane + stearic acid mixture and stearic acid.

runs, where acetic acid was predominant. The diversity of HC species in fluids with 1 to 96 rel.% $H_2O$ (normalised peak areas) exhibited no distinct trends (Fig. 5). The fluids near CW contained $N_2$ as the predominant nitrogen species and trace amounts of nitriles and azines (Supplementary Table 1).

**Calculated $fO_2$ and carbon contents.** Oxygen fugacity ($fO_2$) is the key parameter of fluid systems against which to compare the compositions of fluids synthesised in quenching experiments with data on natural mantle fluids. $fO_2$ in the experimental samples was calculated by Gibbs energy minimisation at 6.3 GPa and 1100–1400 °C knowing the components of the obtained fluids. However, chromatography–mass spectrometry revealed more than 30 carbon and nitrogen species in the fluids, and the calculations required some assumptions. Primarily, the presence of nitrogen species found in very low concentrations was neglected, i.e., the C-O-H-N system was reduced to the C-O-H one. The contribution of alkanes higher than $C_5$, as well as oxygenated hydrocarbons and $CO_2$, all below 1 rel.%, into the $fO_2$ of the system was likewise assumed negligible. With these assumptions, the system composition was simplified to $H_2O$, $CH_4$, $C_2H_6$, $C_3H_8$, and $C_4H_{10}$, and this limited number of main species was used in CG-MS calibrations (see Supplementary information). The normalised peak areas of particular components were converted to mole % only for a part of quenching experiments where equilibrium concentrations of the main components were obtained. They were further used to estimate C contents in the fluids as a function of temperature at constant $fO_2$ and as a function of $fO_2$ at a constant temperature of 1400 °C (Table 7 and Fig. 7). The results generally record markedly lower carbon contents at lower temperatures and higher $fO_2$.

## Discussion

**Processes of fluid equilibration.** According to the reported results, the fluids experimentally generated at 6.3 GPa and 1100–1400 °C attain equilibrium with respect to all C-O-H-N components for the time from 2 to 7 hours. The greatest diversity of carbon species observed in 1-min runs indicates that thermal decomposition of docosane and stearic acid produces numerous non-equilibrium components of the system which disappear in longer runs. GC-MS analysis reveals light alkanes as main run products, with predominant methane and ethane (Table 2). The changes the HCs experience at the experimental conditions can either lengthen or shorten the hydrocarbon chains. For higher hydrocarbons, decomposition most likely occurs as thermal cracking[35] and appears to be the main process involving n-alkanes, including n-docosane and alkyl chains of fatty acids. In principle, the initial thermal formation of radical species from higher hydrocarbons in homolysis and rearrangement reactions leads to further β-scission into alkene and alkyl radicals with shorter chains (Fig. 8a). Ethene that forms in β-scission of terminal radicals in excess of $H_2$ readily reduces to ethane. The radicals resulting from cracking can recombine or react with alkanes or alkenes to form alkanes and new radicals.

Thermal decarboxylation (Fig. 8b) of carboxylic acids (such as stearic acid) produces alkanes shorter for one carbon atom (e.g., relatively high amounts of heptadecane (Supplementary Table 1) in run #1016_7_2) which decompose in a regular way through dehydrogenation and β-scission (Fig. 8a). Catalytic reduction of fatty acids in excess of hydrogen yields primary alcohols. Further dehydration of alcohols to alkenes may be followed by catalytic hydrogenation on the Pt surface producing a mixture of alkanes and terminal alkenes (Fig. 8c).

However, radical reactions of intermediates are also possible at each step of reduction, and varieties of shortened primary alcohols were observed in the experiments. The reactions can be catalysed by Pt, judging by the presence of methanol and ethanol in the fluids from Pt capsules and their absence in the case of Au capsules in 1200 °C runs # 1315_3_5, 1751_2_2 and 1751_2_3 (Supplementary Table 1).

The fluids generated in Au and Pt capsules differ in carbon speciation irrespective of run duration and temperature: methane is one of major fluid components (along with water) in both cases but the methane/ethane ratios of normalised peak areas are, respectively, $CH_4/C_2H_6 > 1$ and $<0.8$ in the Au and Pt capsules (Table 2). This difference may be due to catalytic processes that involve Pt, which may facilitate homolytic dissociation of methane to methyl radicals on the surface at temperatures over 1000 °C[36]. The process accelerates with heating, and the methane/ethane ratio may decrease at higher temperatures. Indeed, the $CH_4/C_2H_6$, $CH_4/C_3H_8$, and $CH_4/C_4H_{10}$ mole ratios we obtained by calibration were the lowest at 1400 °C and at constant $fO_2$ (Fig. 7a). The 7-hr run at 1100 °C gave a spike, possibly, because the system failed to attain equilibrium. Further recombination of the formed radicals produces a mixture of lower HCs: ethane, propane and *n*-butane. The reactivity of ethane is

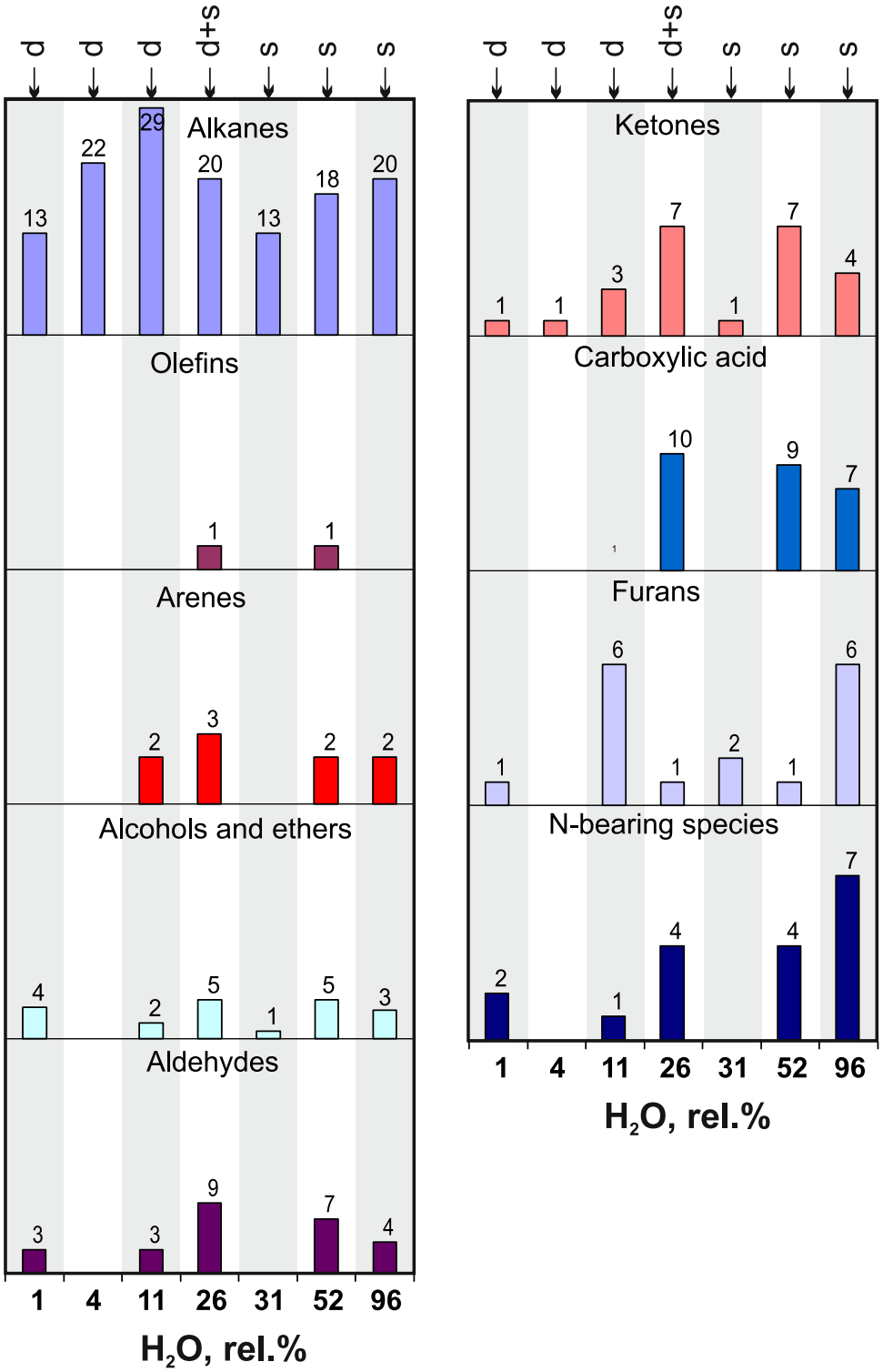


**Figure 5.** Diversity of alkanes, alkenes, and oxygenated hydrocarbons revealed by GC-MS analysis in quenched C-O-H-N fluids as a function of normalised areas of $H_2O$ at 6.3 GPa, 1400 °C, run duration ≥2 hours in MMO-buffered $fH_2$ and in unbuffered experiments. Letter symbols are same as in Fig. 2.

restricted to catalytic dehydrogenation on the Pt surface with formation of ethene, but the excess of hydrogen ($fH_2$ buffered at MMO) impedes this process by shifting the equilibrium toward the reagents. For this reason, ethane does not contribute to the formation of methyl/ethyl radicals and, hence, methane and higher HCs, and tends to accumulate. Nevertheless, the catalytic fission of *n*-butane produces two ethyl radicals that recombine and react with alkenes with further formation of higher HCs.

| Run# | | 1769_2_2 | 1751_2_2 | 1780_2_3 | 1019_7_3 | 1019_7_1 |
|---|---|---|---|---|---|---|
| Capsule | | Pt | Au | Pt | Pt | Pt |
| Temperature (°C) | | 1100 | 1200 | 1300 | 1400 | 1400 |
| Duration (hr) | | 7 | 7 | 7 | 10 | 10 |
| Starting composition* | | Stearic acid + docosane | Stearic acid | Stearic acid | Stearic acid + docosane | Stearic acid |
| Water | | 16.4 | 40.6 | 54.6 | 26.5 | 51.9 |
| Alkanes | $CH_4$ | 35.2 | 37.2 | 13.1 | 17.9 | 17.9 |
| | $C_2H_6$ | 30.8 | 18.2 | 24.0 | 35.3 | 24.6 |
| | $C_3H_8$ | 13.6 | 2.7 | 4.9 | 13.9 | 2.7 |
| | $C_4H_{10}$ | 0.2 | 0.9 | 0.9 | 3.3 | 1.5 |
| | $C_5H_{12}$ | 0.02 | 0.05 | 0.03 | 0.2 | 0.1 |
| | $C_6$-$C_{15}$ | ≤0.04 | ≤0.001 | ≤0.1 | ≤0.04 | ≤0.02 |
| | $C_{15}$–$C_{19}$** | ≤0.9 | ≤0.06 | ≤0.2 | ≤0.02 | ≤0.01 |
| Olefins | — | — | — | ≤0.001 | ≤0.01 | ≤0.01 |
| Arenes | — | — | — | ≤0.003 | ≤0.001 | ≤0.001 |
| Alcohols and ethers | ≤0.2 | ≤0.002 | ≤0.8 | ≤0.01 | ≤0.02 | ≤0.02 |
| Aldehydes | — | ≤0.05 | — | ≤0.003 | ≤0.02 | ≤0.02 |
| Ketones | — | ≤0.01 | — | ≤0.007 | ≤0.01 | ≤0.01 |
| Carboxylic acid | — | <0.001 | ≤0.1 | ≤0.09 | ≤0.02 | ≤0.02 |
| Furans | ≤0.006 | ≤0.001 | ≤0.003 | ≤0.001 | ≤0.01 | ≤0.01 |
| Nitrogen species | | | | | | |
| $N_2$ | 0.4 | 0.02 | 0.08 | 0.01 | 0.01 | 0.01 |
| $CH_3N$ | 0.1 | >1 | — | >1 | 0.9 | 0.9 |

**Table 5.** Representative analyses of quenched $H_2O$-rich C-O-H-N fluids (rel.%) obtained in runs at 6.3 GPa and 1100–1400 °C. *All samples contained graphite. **The quoted concentrations are maximum for a species of the respective group. All GC-MS data are given in Supplementary Table 1.

The fluids generated in both Au and Pt capsules contained various oxygen-bearing compounds, mainly alcohols, ethers, aldehydes, ketones and furans (Tables 4, 5, Supplementary Table 1 and Fig. 3). However, the contents of carbonyl compounds (aldehydes and ketones) were lower in less reduced fluids from Pt samples (Table 5), at comparable T-τ conditions, possibly, because of catalytic hydrogen reduction (Fig. 8d) on the Pt surface and subsequent dehydration of alcohols. The run duration dependence of carbon speciation patterns in Pt capsules (Fig. 1) shows that aldehydes and ketones are the least diverse in the case of 2-hr runs but more diverse in fluids generated in 10-hr runs, possibly, because the catalytical activity of Pt decreases with time.

**Carbon speciation.** Main carbon species in the synthesised equilibrium fluids are $CH_4$, $C_2H_6$, $C_3H_8$ and $C_4H_{10}$, and their concentrations (according to GC-MS analysis) agree well with the calculated relations of $CH_4 > C_2H_6 > C_3H_8 > C_4H_{10}$[20,25,28,32,33] almost in all cases (Fig. 7a,b and Table 7). The $CH_4/C_2H_6$, $CH_4/C_3H_8$, and $CH_4/C_4H_{10}$ ratios are lower in the case of both higher temperature (1400 °C) and $fO_2$ (2.5 log units above IW) at 6.3 GPa (Fig. 7a,b). Taking into account the $H_2O$ variations, this dependence is the reason why temperature and $fO_2$ control the amount of carbon the hydrocarbon fluids can carry (Fig. 7c,d). Previous calculations by Huizenga *et al.* (ref. 25) for 5.0 GPa and 1227 °C gave a similar $fO_2$ dependence of carbon contents in fluids synthesised in the C-O-H system. This similarity indicates that thermodynamic calculations provide a faithful idea of C behaviour in fluids subject to oxidation at CLM pressures. On the other hand, as we have demonstrated experimentally, the amount of carbon in the fluid phase can be notably lower at a lower temperature (1100 °C) at a constant oxygen fugacity of $-\log(fO_2) = 11$.

The equilibrium compositions of the GC-MS analysed C-O-H-N fluids count more than 30 carbon and nitrogen species and contain up to 1 rel.% $C_{15}$-$C_{18}$ alkanes, alcohols, aldehydes, ketones, carboxyl acids, and furans (Tables 4–6 and Figs 1, 3 and 5). In some cases, the contents of species in the obtained fluid vary largely even in runs of the same temperature and starting composition. This variation may result from the presence of moisture that adsorbs, in smaller or larger amounts, on graphite flakes during the capsule assembly. The reduced fluids at $fO_2$ near IW generated by thermal decomposition of docosane are relatively rich only in alcohols, and their composition apparently corresponds to $fO_2$ at which diamonds crystallise from metal melts (ref. 12). At higher $H_2O$, the concentrations of $C_{15}$-$C_{18}$ alkanes increase slightly, while the diversity remains basically the same in alkanes and increases notably in oxygenated hydrocarbons (especially, ketones and carboxylic acids). The effect of lower temperature (1200 °C instead of 1400 °C) is to reduce the diversity of alkanes and oxygenated hydrocarbons in more reduced fluids. As $H_2O$ exceeds 90 mole % and $fO_2$ reaches 2.5 log units above IW, methane in the fluid almost zeroes down, while higher alkanes do not change much (Tables 4–6 and Fig. 5). For instance, the fluids with $fO_2$ near CW contain 1 rel.% $C_2H_6$, fractions of percent $C_3H_8$ and $C_4H_{10}$, and $C_{15-19}$ alkanes, as well as quite large amounts of oxygenated hydrocarbons, especially alcohols and carboxylic acids.

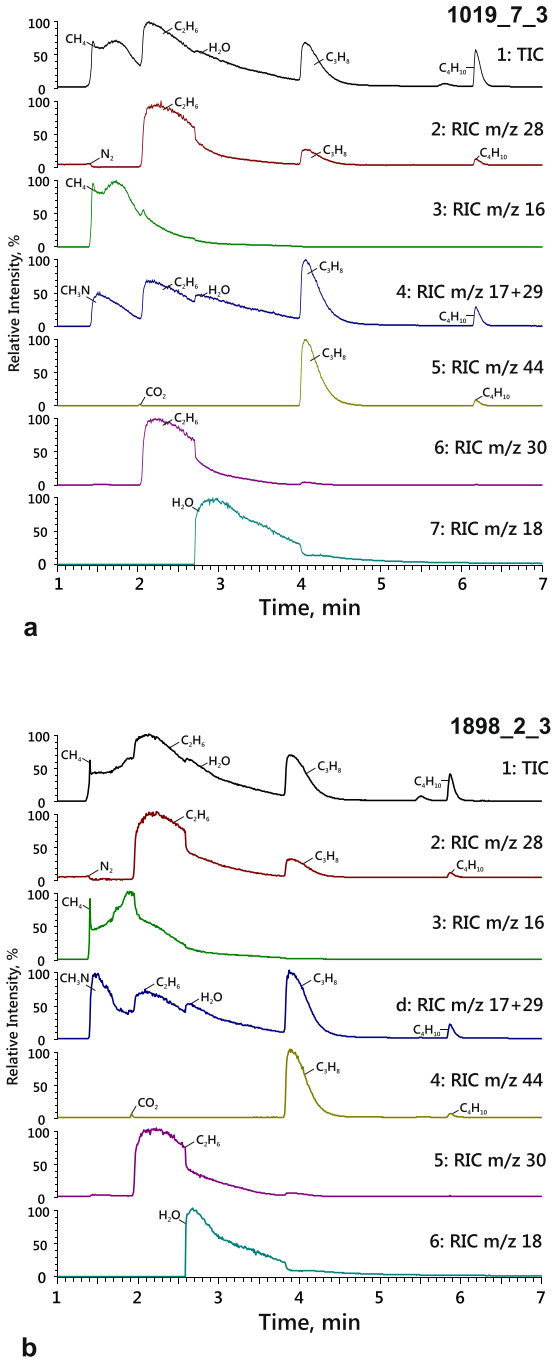


**Figure 6.** Fragments of chromatograms of quenched fluids extracted from Pt capsules after runs 1019_7_3 (**a**) and 1898_2_3 (**b**). 1 = Total ion current (TIC) chromatograms; 2 = Reconstructed ion chromatograms (RIC) m/z 28 that characterise traces of molecular nitrogen, ethane, propane and butane; 3 = RIC m/z 16: methane; 4 = RIC m/z 17 + 29: methanimine; 5 = RIC m/z 44: traces of carbon dioxide, propane and butane; 6 = RIC m/z 30: ethane; 7 = RIC m/z 18: water.

The effect of Pt and Au capsules on the composition of equilibrium C-O-H-N fluids is seen in the results of 7-hr long runs at 1100–1300 °C (Table 2 and Fig. 3) where $CH_4/C_2H_6$ in the fluids from Au capsules are higher than with Pt capsules (Table 2) which become involved in catalytic processes (see above). Fluids generated in the two types of capsules are similar in diversity of alkanes (Fig. 4), while $H_2O$-rich fluids from Pt capsules have low or absent aldehydes and ketones, possibly, due to catalytic hydrogen reduction at the Pt surface, and subsequent dehydration of the formed alcohols. The composition similarity of the quenched fluids synthesised in Pt and Au capsules indicates that the Pt effect consists in faster attainment of equilibrium in the system and must be the smallest in 10-hr runs.

| Run# | | 1315_3_5 | 1720_2_2 |
|---|---|---|---|
| Capsule | | Pt | Pt |
| Temperature (°C) | | 1200 | 1400 |
| Duration (hr) | | 7 | 7 |
| Starting composition* | | Stearic acid | Stearic acid |
| Water | | 93.5 | 96.3 |
| Alkanes | $CH_4$ | 2.9 | 0.06 |
| | $C_2H_6$ | 0.7 | 1.4 |
| | $C_3H_8$ | 0.4 | 0.08 |
| | $C_4H_{10}$ | 1.0 | 0.8 |
| | $C_5H_{12}$ | 0.02 | 0.1 |
| | $C_6$-$C_{14}$** | — | ≤0.08 |
| | $C_{15}$-$C_{19}$ | ≤0.04 | ≤0.2 |
| Olefins | | — | — |
| Arenes | | — | ≤0.008 |
| Alcohols and ethers | | ≤0.7 | ≤0.01 |
| Aldehydes | | ≤0.003 | ≤0.01 |
| Ketones | | — | ≤0.01 |
| Carboxylic acid | | ≤0.008 | <0.07 |
| Furans | | ≤0.006 | ≤0.01 |
| Nitrogen species | | | |
| $N_2$ | | 0.5 | 0.01 |
| $CH_3N$ | | — | — |

**Table 6.** Representative analyses of quenched $H_2O$-rich C-O-H-N fluids (rel.%) obtained in unbuffered runs at 6.3 GPa. *All samples contained graphite. **The quoted concentrations are maximum for a species of the respective group. All GC-MS data are given in Supplementary Table.

| Run# | Capsule | Buffer $fH_2$ | T, (°C) | Calc. $fO_2$ | $CH_4/C_2H_6$ | $CH_4/C_3H_8$ | $CH_4/C_4H_{10}$ | C, mole % |
|---|---|---|---|---|---|---|---|---|
| 1769_2_2 | Pt | MMO | 1100 | −10.8 | 20 | 5.1 | 10.8 | 3.0 |
| 1315_3_5 | Pt | — | 1200 | −8.5 | 227 | 1384 | 839 | 0.01 |
| 1751_2_2 | Au | MMO | 1200 | −10.8 | 2012 | 14912 | 47973 | 8.7 |
| 1751_2_3 | Pt | MMO | 1200 | −15.4 | 2774 | 18853 | 59694 | 19.9 |
| 1746_2_3 | Pt | MMO | 1300 | −9.0 | 22 | 109 | 237 | 6.3 |
| 1746_2_2 | Pt | MMO | 1300 | −10.5 | 2063 | 36898 | 85957 | 14.1 |
| 1780_2_2 | Pt | MMO | 1300 | −9.3 | 6.9 | 8.7 | 17 | 8.9 |
| 1780_2_3 | Pt | MMO | 1300 | −8.5 | 5.7 | 2.8 | 5.8 | 4.9 |
| 1753_2_3 | Pt | MMO | 1400 | −10.6 | 433 | 2412 | 4733 | 18.3 |
| 1898_2_1 | Pt | MMO | 1400 | −10.5 | 224 | 1677 | 4297 | 18.2 |
| 1898_2_3 | Pt | MMO | 1400 | −10.9 | 244 | 1181 | 4804 | 18.8 |
| 1720_2_2 | Pt | — | 1400 | −6.0 | 5.7 | 6.7 | 11.1 | 0.01 |
| 1727_2_2 | Pt | MMO | 1400 | −8.8 | 26 | 12 | 24.98 | 12.6 |
| 1019_7_1 | Pt | MMO | 1400 | −8.1 | 176 | 2016 | 3471 | 7.3 |
| 1019_7_3 | Pt | MMO | 1400 | −11.0 | 274 | 1711 | 4797 | 18.9 |

**Table 7.** Mole ratios of $CH_4$, $C_2H_6$, $C_3H_8$ and $C_4H_{10}$, carbon content (mole %), and calculated $fO_2$ in fluid phase, according to GC-MS calibration (see text for explanation).

All detected carbon species, except alkanes, turn out to be very sensitive to cooling rates: they are much more diverse at slow (1 deg/s) cooling (Fig. 1). Therefore, back reactions upon cooling lead primarily to synthesis of oxygenated hydrocarbons.

**Nitrogen speciation.** Nitrogen in the studied C-O-H-N fluids is mainly air $N_2$ entrapped by the capsule assembly, which reacts with hydrogen, hydrocarbons, and graphite at the experiment *P-T* conditions to form methanimine (Table 2, Figs 6 and 8): $CH_3N$ with the formula  . The fluids also contain trace amounts of other nitrogen species, such as some nitriles, mainly at 1400 °C and high $H_2O$ contents. $CH_3N/N_2$ ratios estimated by GC-MS (Fig. 9) show that $CH_3N$ is the main nitrogen species in almost all equilibrium reduced fluids; $CH_3N/$

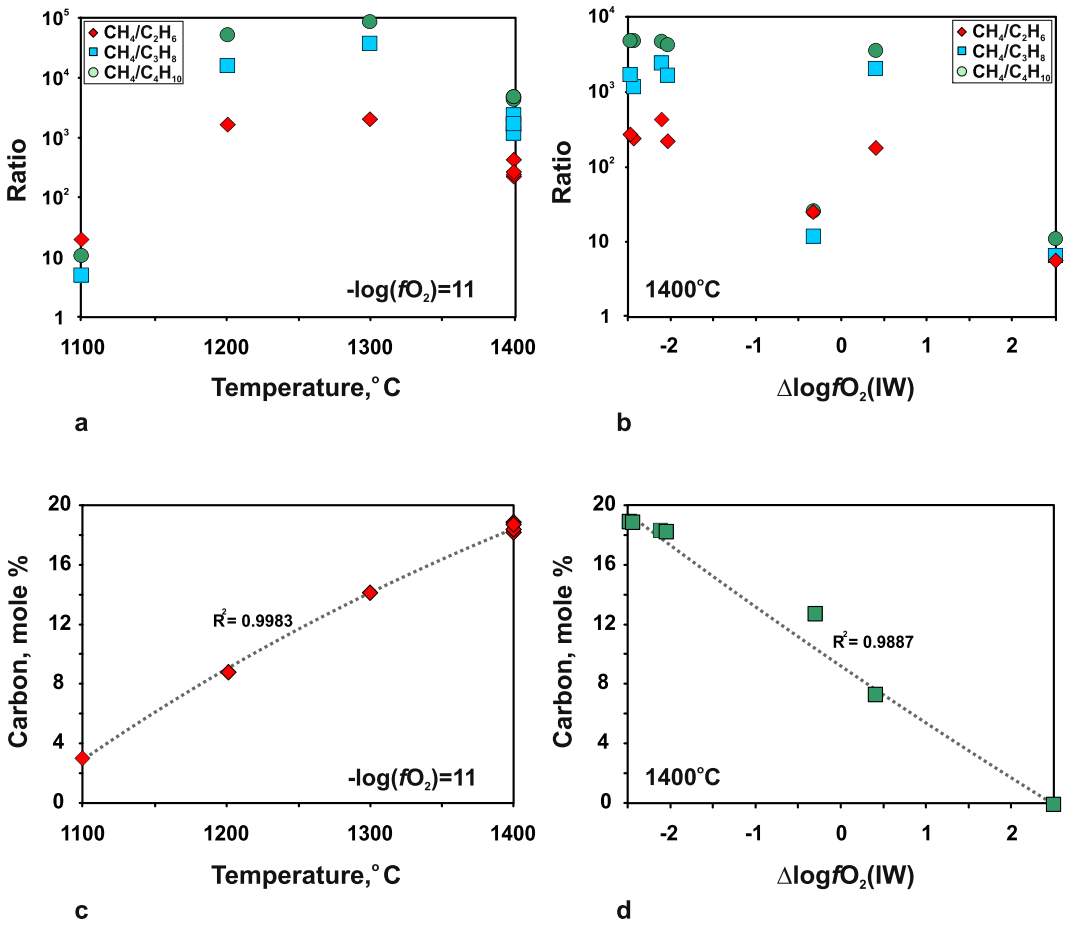


**Figure 7.** Composition of quenched fluids converted using GC-MS calibration with respect to main species: $CH_4$, $C_2H_6$, $C_3H_8$, $C_4H_{10}$ and $H_2O$. a: mole ratios $CH_4/C_2H_6$, $CH_4/C_3H_8$ and $CH_4/C_4H_{10}$ in strongly reduced fluids at 6.3 GPa, 1100–1400 °C and constant $fO_2$; b: same at 6.3 GPa, 1400 °C in a range of $fO_2$; c: amount of carbon in fluids as a function of temperature; d: amount of carbon in fluids as a function of $fO_2$.

$N_2 < 1$ only at 1100 °C and $fO_2$ about −11 log units. However, $CH_3N$ disappears at 1400 °C when $fO_2$ becomes four orders of magnitude higher and approaches CW. The temperature and redox dependence of $CH_3N$ stability (with regard to the slope of buffers in the T-$fO_2$ diagram of Fig. 10) indicates that the formation of $CH_3N$ is possible at low $fO_2$.

Thus, $CH_3N$ discovered in the C-O-H-N system at 6.3 GPa, 1100–1400 °C, and a fluid C/N ratio of ~20 may be an important component in reduced mantle containing minor amounts of nitrogen. It may predominate as a nitrogen host already at $fO_2$ near and below IW. A more detailed study is obviously required to constrain the stability of $CH_3N$ at the mantle *P-T-*$fO_2$ conditions, with a special focus on nitrogen sources in the reactions that produce this species. Note that $NH_3$ and $N_2$ are stable in the N-rich C-O-H-N system generated by decomposition of melamine, as well as its mixture with stearic acid or docosane at C/N ratio in the fluid from 0.4 to 4.6, at similar *P-T-*$fO_2$[34], while the redox stability of $CH_3N$ is comparable with that of ammonia[3,34]. To sum up, the behaviour of $CH_3N$ may control the deep nitrogen cycle in N-poor reduced peridotitic mantle. Specifically, silicate phases capable of dissolving ammonia in the presence of $NH_3$-bearing fluids[2,19,37] hardly can host nitrogen in equilibrium with $CH_3N$-bearing mantle fluids.

**Carbon and nitrogen transport across redox and thermal barriers in the mantle.** The most important carbon and nitrogen species of C-O-H-N fluids in the upper mantle revealed in this study of N-poor fluids, as well as in previous results for N-rich fluids[34], are $CH_4$ and $CH_3N$ in the depleted domains with ~20 ppm C and ~1 ppm N[38,39], and $CH_4$ and $NH_3$ in the enriched domains containing ~250 ppm C and ~100 ppm N[38,39] (Fig. 11). Note that this inference is based on experiments with a simplified C-O-H-N system limited to four components, whereas the speciation in the natural mantle fluids is much more complex. Namely, N-rich fluids derived from a subducting slab may be quite rich in chlorides[40]. The appearance of the $Cl^-$ ion in the fluid may be coupled to $NH_4^+$ forming a stable ligand. Furthermore, the real fluid phase in the mantle occurs in the interstitial space of silicate rocks. As it was shown previously[6], the pH values of the eclogitic fluids are strongly alkaline, which supports the model of ionic C-bearing species. At the same time, fluids in equilibrium with mantle peridotite minerals generally contain species in the molecular form[6], which is consistent with the conventional fluid models.

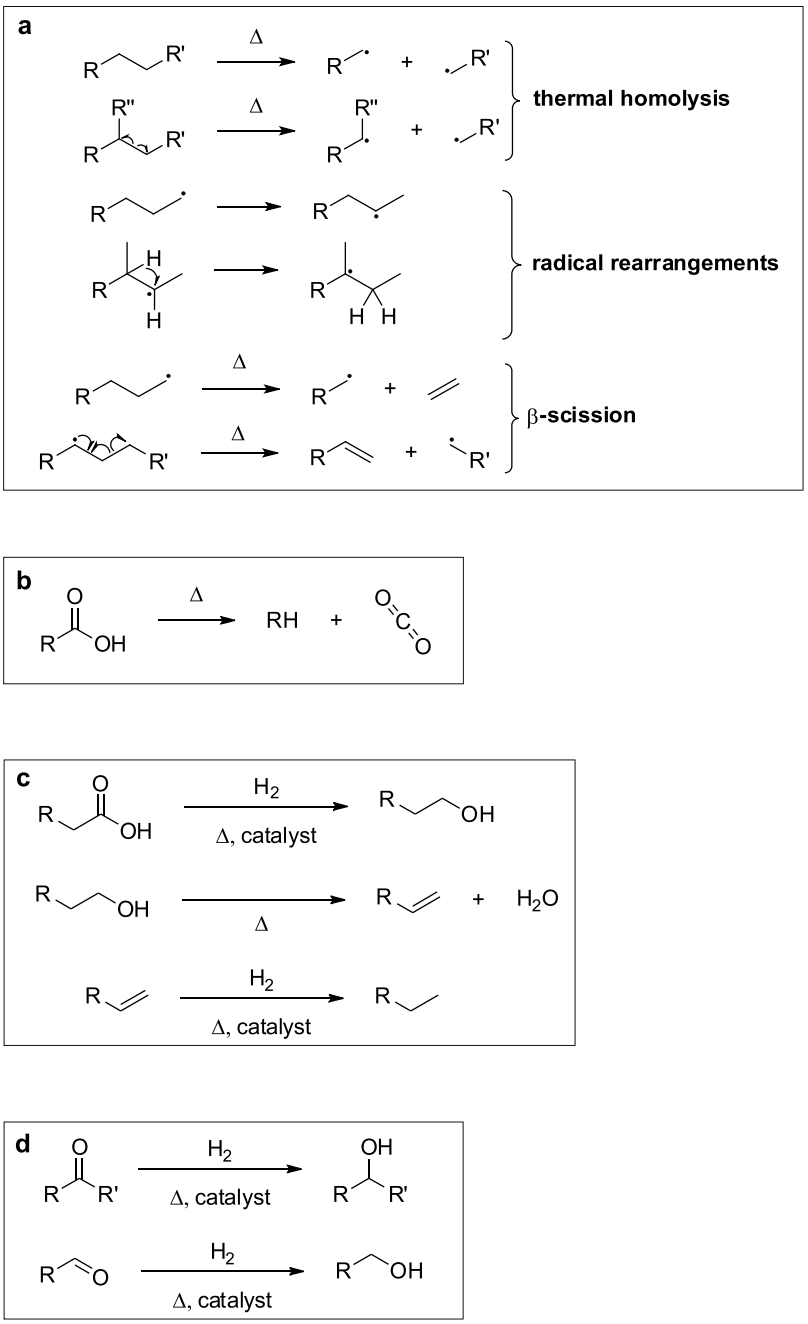


**Figure 8.** Main chemical processes during formation of equilibrium fluids. (**a**) initial thermal formation of radical species from higher hydrocarbons in homolysis, rearrangement, their further rearrangement and β-scission reactions; (**b**) thermal decarboxylation of carboxylic acids; (**c**) processes involving carboxyl acids; (**d**) hydrogen reduction of carbonyl compounds.

The ascent of N-bearing reduced fluids is an important element of the carbon and nitrogen cycles in the mantle[2,5]. On their way to shallow mantle, these fluids can cross redox and/or temperature barriers, such as multiple redox fronts[24] in the lithosphere or the boundary between hotter asthenosphere and colder lithosphere[41]. Our experiments and published calculation results[20,25,28,32,33] have implications for the behaviour of fluids crossing such redox and thermal barriers. Carbon concentrations in reduced fluids within the $T$-$fO_2$ range of CLM at a depth of ~200 km vary as plotted in Fig. 10. The reduced fluids stable at ~IW lose almost all carbon (about 18 mole % C, Figs 7e and 10) upon isothermal oxidation at 1400 °C to $fO_2$ about CW. For the fluids with methane as a predominant carbon species, the experimentally obtained and calculated[25] for 5.0 GPa and 1227 °C amounts of carbon released during oxidation are in good agreement. The novelty of the experimental results is that HCs show different degrees of stability to oxidation, and this difference can affect the carbon speciation in the fluid. Namely, oxidation can be expected to decrease the concentrations of methane and ethane (much more strongly for the former) but to cause almost no effect on $C_3$, $C_4$ and $C_5$ alkanes (Table 2 and Fig. 7b), as well as on some $C_{15}$-$C_{19}$

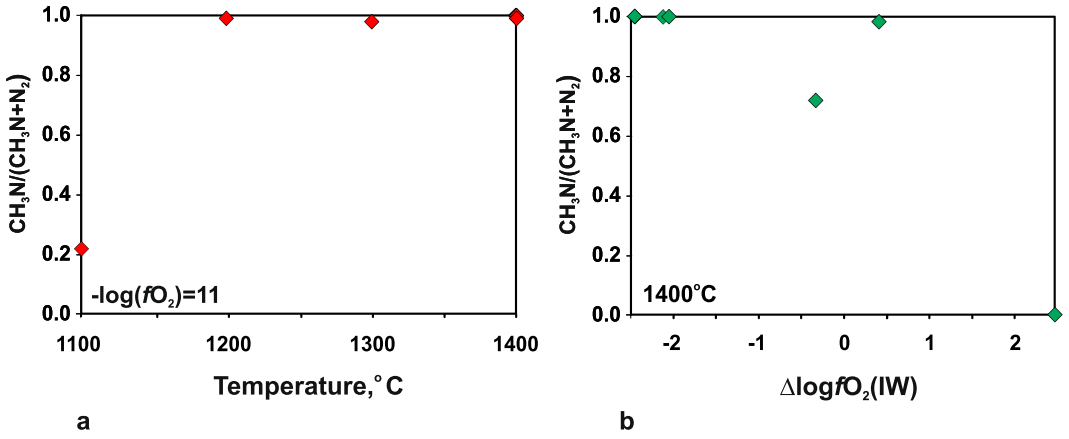


**Figure 9.** Normalised peak area ratios of $CH_3N$ and $N_2$ that characterise their role as nitrogen species in C-O-H-N fluids in a large range of *T*-$fO_2$ parameters at 6.3 GPa. (**a**) 1100–1400 °C and constant $fO_2$; (**b**) redox interval from strongly to moderately reduced conditions.

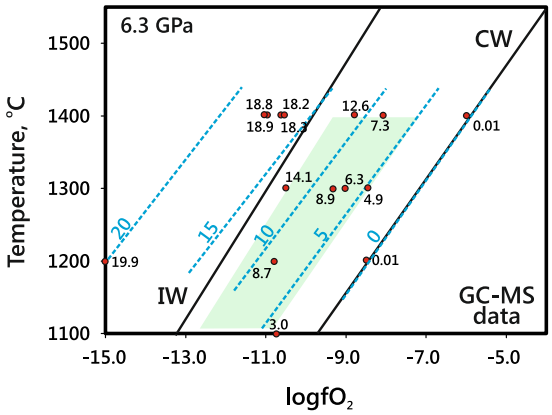


**Figure 10.** Concentrations of carbon (mole %) in reduced C-O-H-N fluids at 6.3 GPa, according to GC-MS analysis. Red circles are GC-MS-measured values for experimental compositions; blue dash line is the carbon isopleth. Light-green field shows T-$fO_2$ range for cratonic lithospheric mantle at a depth of ~200 km (see text for explanation). IW and CW curves are after refs 1, 24 and 56.

alkanes which remain within fractions of percent (Table 6). Note also that $H_2O$-rich fluids at 1400 °C contain diverse oxygenated hydrocarbons (Fig. 5), with predominant acetic acid. As for nitrogen species, we infer $CH_3N$ to become less important and the role of $N_2$ to grow as oxidation progresses (Fig. 9b).

The question whether any hydrocarbons can survive transport across the mantle redox fronts is essential for understanding the deep carbon cycle. Neither the stability of higher alkanes at $fO_2$ near CW nor the oxidation patterns of hydrocarbon fluids have been studied experimentally at mantle *P*-*T* conditions. In our previous quenching experiments with anthracene ($C_{14}H_{10}$), performed without external $fH_2$ buffering[31], oxidation of the C-O-H system produced an aqueous fluid with trace amounts of $CH_4$ (0.5 to 0.7 mole%) and $C_2H_6$ ($\leq$0.1 mol.%). According to the data of this study, hydrous silicate magmas generated within multiple redox fronts can entrap minor amounts of some higher alkanes and oxygenated hydrocarbons of mantle origin and carry them further to shallow mantle.

As modeling by Stachel and Luth (ref. 5) demonstrates, less than 50 ppm fluid are required to completely reset the redox state of depleted cratonic peridotite to that of the fluid. Taking into account the strongly reduced chemistry of most peridotites at the depths of diamond stability[20–23], Stachel and Luth (ref. 5) conclude that redox fronts can be unstable to interaction with hydrocarbon fluids and that the last fluids to interact with the deep CLM are generally reducing. The fluids which penetrate into reduced but colder CLM domains and cool down from 1400 °C and $fO_2$ ~IW to 1100 °C at $fO_2$ slightly above IW are inferred to loose carbon (decreasing from 18 to 3 mole %) but gain water (Figs 7a,c and 10). The cooled fluids contain more ethane, propane, and butane but much less diverse oxygenated hydrocarbons, mainly methanol and ethanol (Fig. 3 and Table 5, Supplementary Table 1). As for nitrogen speciation, $N_2$ is expected to be predominant instead of $CH_3N$ ($CH_3N/N_2 < 1$) (Fig. 9a) in the cooled peridotitic fluid, which contains mainly molecular forms of species.

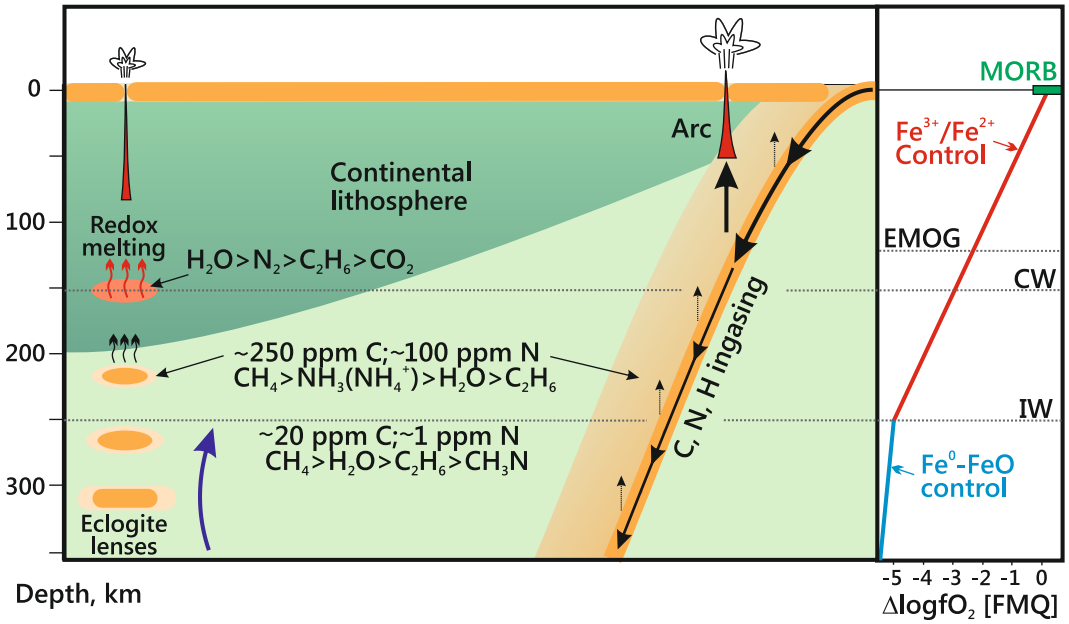


**Figure 11.** Schematic of the upper mantle volatile cycle and main carbon and nitrogen species of C-O-H-N fluids in depleted and enriched domains[38,39]. Black arrows show paths and estimates of the relative magnitudes of carbon, nitrogen and hydrogen fluxes and blue arrow is mantle upwelling. Right panel: potential mantle $fO_2$ as a function of depth. The $Fe^0$-FeO and $Fe^{3+}/Fe^{2+}$ (equilibria involving the exchange of $Fe^{3+}$ and $Fe^{2+}$ between silicate minerals) curves are according to refs 1 and 56. Oxygen fugacity of CW (maximum $H_2O$ content in C-O-H fluids), EMOD/G (equilibria enstatite + magnesite = olivine + graphite/diamond) and MORB (mid-ocean ridge basalts) are according to refs 1 and 24. 'Redox melting' process at depths of 120–150 km is according to refs 1 and 24.

**Diamond formation.** Carbon-bearing fluids in CLM can act as both carbon carriers and diamond crystallisation environment[5,42–45]. The reaction of hydrocarbons with $O_2$ at multiple redox fronts[24] stimulates the activity of $H_2O$ and causes drastic reduction of total carbon content in the fluids, as well as rapid drop in the solidus temperature of the ambient rocks. The redox melting is considered to be an important process in the cratonic mantle lithosphere[24]. As a result of oxidation, carbon of methane and other hydrocarbons is inferred to release in the form of $C^0$ and to become consumed for saturation with the aqueous fluid. Experimental data show that this $C^0$ could be involved in diamond crystallisation. The chemistry of mineral inclusions in diamond[46,47] and stable isotope data of carbon and nitrogen[48] indicate distinct possibility of diamond precipitation from $CH_4$. Higher alkanes and some oxygenated hydrocarbons have been shown experimentally to be stable against oxidation of hydrocarbon fluids till the water maximum (Table 6). Therefore, they should be present in the diamond crystallisation environment, along with water, and can be entrapped as inclusions. Recent studies[8–11] confirm the presence of higher HCs in inclusions from diamond and its syngenetic mantle-derived minerals.

The available experimental data on crystallisation of diamond from the fluid phase[49–53] indicate the existence of important, possibly, kinetic barriers impeding its spontaneous nucleation and further growth in the mantle fluid. Diamond has never been synthesised from strongly reduced fluids in the field of its thermodynamic stability, even in the presence of metastable graphite[31,52]. Note that none of our experiments, from 1 minute to 10 hours long, led to spontaneous diamond nucleation, even near CW. As we showed earlier[31], diamond can nucleate and grow at run duration at least 40 hours, at 1600 °C and at relatively high $fO_2$ near CW, in $H_2O$-rich fluids. At lower temperatures, diamond nucleation begins even in oxidised carbonatitic fluids after a much longer induction period[44,51,54]. Thus, only oxidation of fluids within redox fronts at temperatures approaching 1400 °C can maintain effective diamond formation. Fluids cooling in strongly reduced mantle can release excess carbon as metastable graphite. The fate of this graphite within CLM may be different: it may either remain in the metastable state for an infinitely long time or convert to diamond upon interaction with oxidised alkaline metasomatic fluids[44,51,54]. This mechanism is similar to the model suggested by Jablon and Navon (ref. 55) as universal for most diamonds from CLM.

## Conclusions

Experiments at 6.3 GPa show that fluids generated by thermal decomposition of docosane and stearic acid can attain equilibrium for 2 and 7 hours at 1400 and 1100 °C, respectively. The shortest 1-min runs lead to the formation of numerous non-equilibrium components of the system, especially oxygenated hydrocarbons which disappear in longer runs. The processes leading to equilibrium are mainly radical and include thermal formation of radical species from higher hydrocarbons and carboxylic acids in homolysis, rearrangement reactions, and further β-scission into alkenes and alkyl radicals. Carboxylic acids additionally undergo thermal decarboxylation. Equilibrium fluids contain $CH_4$, $C_2H_6$, $C_3H_8$ and $C_4H_{10}$ as main carbon species, which is consistent with previous

experimental and theoretical results[25, 28, 29, 31, 32]. It has been demonstrated for the first time that equilibrium N-poor C-O-H-N fluids can contain more than 30 carbon and nitrogen species. Besides the main species, they include $C_{15}$-$C_{19}$ alkanes, alcohols, aldehydes, ketones, carboxylic acids, and furans.

The carbon and nitrogen speciation in the equilibrium fluids depends on temperature and redox conditions. The $CH_4/C_2H_6$, $CH_4/C_3H_8$, and $CH_4/C_4H_{10}$ ratios and C concentrations decrease both under isobaric cooling from 1400 to 1200 °C at constant $fO_2$ and under oxygen fugacity increase from IW-2.5 to IW + 2.5 log units at 1400 °C. As the temperature and water content increase, the concentrations of $C_{15}$-$C_{18}$ alkanes increase slightly while oxygenated hydrocarbons become more diverse. In reduced fluids, only alcohols can reach notable amounts. The fluids with $fO_2$ IW + 2.5 log units, almost lack methane and contain about 1 rel.% of $C_2H_6$, $C_3H_8$ and $C_4H_{10}$, as well as $C_{15-19}$ alkanes, and relatively high oxygenated hydrocarbons, especially alcohols and carboxylic acids. The material of capsules causes a catalytic effect: $CH_4/C_2H_6$ ratios are slightly higher in quenched fluids from Au capsules than in those from Pt capsules. Methanimine ($CH_3N$) is the main nitrogen species in the studied fluids, but it loses importance ($CH_3N/N_2 < 1$) at a lower temperature of 1100 °C at constant $fO_2$ in the system IW-2.5 log units; $CH_3N$ almost disappears while $N_2$ becomes the predominant species as $fO_2$ decreases to IW + 2.5 log units at 1400 °C.

The behaviour of the $CH_3N$ species can strongly control the mantle nitrogen cycle, especially in N-poor fluids equilibrated with peridotite. Specifically, silicate phases capable of dissolving ammonia in the presence of $NH_3$-bearing fluids hardly can be nitrogen hosts in equilibrium with $CH_3N$-bearing fluids. Oxidation of peridotitic fluids with small N contents upon interaction with multiple redox fronts is inferred to decrease strongly the concentrations of methane and methanimine and slightly reduce the amount of ethane, but it causes significant changes neither to $C_3$, $C_4$ and $C_5$ alkanes nor to $C_{15}$-$C_{19}$ alkanes and oxygenated hyrocarbons. As a result, hydrous magma can capture species stable to oxidation, as well as $N_2$, which can be involved in diamond formation and carried to shallow mantle.

## Materials and Methods

Starting mixtures for generation of carbon- and nitrogen-bearing fluids consisted of chemical-grade docosane ($C_{22}H_{46}$) and stearic acid ($C_{18}H_{36}O_2$), and 99.9999% pure natural graphite (Table 1). The pre-dried graphite contained 700 ppm $CO_2$ and 700 ppm $H_2O$ determined by chromatography of gases extracted during graphite annealing at 600 °C in a U-shaped quartz cell. Graphite with docosane and/or stearic acid, at a weight ratio of ~10/1, were placed into Pt or Au capsules (Supplementary Fig 1). The 10/1 ratio of graphite to fluid-generating material provided an amount of C-O-H-N fluid sufficient for GC/MS analysis but did not produce overpressure in the capsule after the runs and during drying before gas analysis. Microscopic amounts of nitrogen in the capsules came from air. The samples had different $H_2O$ concentrations changed by varying the aliquots of stearic acid. Capsules containing starting material for the generation of a C-O-H-N fluid were arc-welded using a *Lampert Werktechnik GmbH* PUK-4U impulse micro welding device. Experiments were carried out in a high-pressure split-sphere multi-anvil apparatus. Fluid was generated at buffered $fH_2$ in 6.3 GPa runs in a cell with a large low-gradient zone and was analyzed using a Thermo Scientific *DSQ II Series Dual Stage Quadrupole GC/MS*[34]. Analytical uncertainty for $H_2O$, $NH_3$, and $CO_2$, expressed as precision, was less than 10% and in most cases less than 5% (determined in the range from 12.5 pptv to 12.5 ppbv). The efficiency of the chosen $fH_2$ buffering technique has been proven in special tests (Supplementary Figs 1–3).

## References


1. Stagno, V., Ojwang, D. O., McCammon, C. A. & Frost, D. J. The oxidation state of the mantle and the extraction of carbon from Earth's interior. *Nature* **493**, 84–88 (2013).
2. Luth, R. W. Volatiles in Earth's mantle. *Treatise on Geochemistry* 3.9, (355–391. Elsevier: Oxford, 2014).
3. Li, Y. & Keppler, H. Nitrogen speciation in mantle and crustal fluids. *Geochim. Cosmochim. Acta* **129**, 13–32 (2014).
4. Smith, E. M. & Kopylova, M. G. Implications of metallic iron for diamonds and nitrogen in the sub-lithospheric mantle. *Can. J. Earth Sci.* **51**, 510–516 (2014).
5. Stachel, T. & Luth, R. W. Diamond formation - Where, when and how? *Lithos* **220–223**, 200–220 (2015).
6. Sverjensky, D. A., Stagno, V. & Huang, F. Important role for organic carbon in subduction-zone fluids in the deep carbon cycle. *Nature Geoscience* **7**, 909–913 (2014).
7. Sugisaki, R. & Mimura, K. Mantle hydrocarbons: abiotic or biotic? *Geochim. Cosmochim. Acta* **58**, 2527–2542 (1994).
8. Tomilenko, A. A., Ragozin, A. L., Shatskii, V. S. & Shebanin, A. P. Variation in the fluid phase composition in the process of natural diamond crystallization. *Doklady Earth Sciences* **379**, 571–574 (2001).
9. Tomilenko, A. A., Kovyazin, S. V., Pokhilenko, L. N. & Sobolev, N. V. Primary hydrocarbon inclusions in garnet of diamondiferous eclogite from the Udachanaya kimberlite pipe, Yakutia. *Doklady Earth Sciences* **426**, 695–698 (2009).
10. Tomilenko, A. A., Bul'bak, T. A., Pokhilenko, L. N., Kuzmin, D. V. & Sobolev, N. V. Peculiarities of the composition of volatile components in picroilmenites from Yakutian kimberlites of various ages (by gas chromatography—mass spectrometry). *Doklady Earth Sciences* **469**, 690–694 (2016).
11. Sobolev, N. V. *et al*. Mineral and fluid inclusion in the diamonds from the Ural placers, Russia. *AGU Fall Meeting*. San Francisco, 14–18 December (2015).
12. Smith, E. M., Shirey, S. B., Nestola, F., Bullock, E. S., Wang, J., Richardson, S. H. & Wang, W. Large gem diamonds from metallic liquid in Earth's deep mantle. *Science* **354**, 1403–1405 (2016).
13. Chekaliuk, E. B. Thermodynamic Background for the Theory of Abiotic Petroleum Genesis. Naukova Dumka, Kiev (1971). (in Russian).
14. Ancilotto, F., Chiarotti, G. L., Scandolo, S. & Tosatti, E. Dissociation of methane into hydrocarbons at extreme (planetary) pressure and temperature. *Science* **275**, 1288–1290 (1997).
15. Karpov, I. K., Chudnenko, K. V. & Kulik, D. A. Modeling chemical mass-transfer in geochemical processes: thermodynamic relations, conditions of equilibria and numerical algorithms. *Am. J. Sci.* **297**, 767–806 (1997).
16. Kenney, J. F., Kutcherov, V. A., Bendeliani, N. A. & Alekseev, V. A. The evolution of multicomponent systems at high pressures: VI. The thermodynamic stability of the hydrogen– carbon system: the genesis of hydrocarbons and the origin of petroleum. *Proceedings of the National Academy of Sciences* **99**, 10976–10981 (2002).

17. Spanu, L., Donadio, D., Hohl, D., Schwegler, E. & Galli, G. Stability of hydrocarbons at deep Earth pressures and temperatures. *Proceedings of the National Academy of Sciences* **108**, 6843–6846 (2011).
18. Watenphul, A., Wunder, B., Wirth, R. & Heinrich, W. Ammonium-bearing clinopyroxene: A potential nitrogen reservoir in the Earth's mantle. *Chem. Geol.* **270**, 240–248 (2010).
19. Li, Y., Wiedenbeck, M., Shcheka, S. & Keppler, H. Nitrogen solubility in upper mantle minerals. *Earth Planet. Sci. Lett.* **377**, 311–323 (2013).
20. Woodland, A. B. & Koch, M. Variation in oxygen fugacity with depth in the upper mantle beneath the Kaapvaal craton, Southern Africa. *Earth Planet. Sci. Lett.* **214**, 295–310 (2003).
21. McCammon, C. & Kopylova, M. G. A redox profile of the Slave mantle and oxygen fugacity control in the cratonic mantle. *Contrib. Mineral. Petrol.* **148**, 55–68 (2004).
22. Goncharov, A. G., Ionov, D. A., Doucet, L. S. & Pokhilenko, L. N. Thermal state, oxygen fugacity and C-O-H fluid speciation in cratonic lithospheric mantle: new data on peridotite xenoliths from the Udachnaya kimberlite, Siberia. *Earth Planet. Sci. Lett.* **357**, 99–110 (2012).
23. Yaxley, G. M., Berry, A. J., Kamenetsky, V. S., Woodland, A. B. & Golovin, A. V. An oxygen fugacity profile through the Siberian Craton — Fe K-edge XANES determinations of $Fe^{3+}/\Sigma Fe$ in garnets in peridotite xenoliths from the Udachnaya East kimberlite. *Lithos* **140**, 142–151 (2012).
24. Foley, S. F. A reappraisal of redox melting in the Earth's mantle as a function of tectonic setting and time. *J. Petrol.* **52**, 1363–1391 (2011).
25. Huizenga, J. M., Crossingham, A. & Viljoen, F. Diamond precipitation from ascending reduced fluids in the Kaapvaal lithosphere: thermodynamic constraints. *Comptes Rendus Géoscience* **344**, 67–76 (2012).
26. Mikhail, S. & Sverjensky, D. A. Nitrogen speciation in upper mantle fluids and the origin of Earth's nitrogen-rich atmosphere. *Nature Geoscience* **7**, 816–819 (2014).
27. Sverjensky, D. A. & Huang, F. Diamond formation due to a pH drop during fluid–rock interactions. *Nature Communication*, doi: 10.1038/ncomms9702 (2015).
28. Taylor, W. R. & Foley, S. F. Improved oxygen-buffering techniques for C–O–H fluid-saturated experiments at high pressure. *J. Geophys. Res.* **94**, 4146–4158 (1989).
29. Matveev, S., Ballhaus, C., Fricke, K., Truckenbrodt, J. & Ziegenbein, D. Volatiles in the Earth's mantle: I. Synthesis of CHO fluids at 1273 K and 2.4 GPa. *Geochim. Cosmochim. Acta* **61**, 3081–3088 (1997).
30. Sokol, A. G., Pal'yanov, Y. N., Pal'yanova, G. A. & Tomilenko, A. A. Diamond crystallization in fluid and carbonate–fluid systems under mantle P–T conditions: 1. *Fluid composition. Geochem. Int.* **42**, 830–838 (2004).
31. Sokol, A. G., Palyanova, G. A., Palyanov, Y. N., Tomilenko, A. A. & Melenevsky, V. N. Fluid regime and diamond formation in the reduced mantle: experimental constraints. *Geochim. Cosmochim. Acta* **73**, 5820–5834 (2009).
32. Kadik, A. Evolution of Earth's redox state during upwelling of carbon-bearing mantle. *Phys. Earth Planet. Inter.* **100**, 157–166 (1997).
33. Simakov, S. K. Redox state of eclogites and peridotites from sub-cratonic upper mantle and a connection with diamond genesis. *Contrib. Mineral. Petrol.* **151**, 282–296 (2006).
34. Sokol, A. G., Palyanov, Y. N., Tomilenko, A. A., Bul'bak, T. A. & Palyanova, G. A. Carbon and nitrogen speciation in nitrogen-rich C-O-H-N fluids at 5.5–7.8 GPa. *Earth Planet. Sci. Lett.* **460**, 234–243 (2017).
35. Sadeghbeigi, R. Fluid catalytic cracking handbook: An expert guide to the practical operation, design, and optimization of FCC units. Elsevier (2012).
36. Robertson, A. J. B. The Pyrolysis of Methane, Ethane and n-butane on a Platinum Filament. In *Proceedings of the Royal Society of London A: Mathematical, Physical and Engineering Sciences* (Vol. 199, No. 1058, pp. 394–411) The Royal Society (1949).
37. Watenphul, A., Wunder, B. & Heinrich, W. High-pressure ammonium-bearing silicates: Implications for nitrogen and hydrogen storage in the Earth's mantle. *Am. Mineral.* **94**, 283–292 (2009).
38. Marty, B. The origins and concentrations of water, carbon, nitrogen and noble gases on Earth. *Earth Planet. Sci. Lett.* **313–314**, 56–66 (2012).
39. Dasgupta, R. & Hirschmann, M. M. The deep carbon cycle and melting in Earth's interior. *Earth Planet. Sci. Lett.* **298**, 1–13 (2010).
40. Weiss, Y., McNeill, J., Pearson, D. G., Nowell, G. M. & Ottley, C. J. Highly saline fluids from a subducting slab as the source for fluid-rich diamonds. *Nature* **524**, 339–342 (2015).
41. Pearson, D. G. & Wittig, N. The formation and evolution of cratonic mantle lithosphere - Evidence from mantle xenoliths. *Treatise on Geochemistry* **2**, 255–292 (2014).
42. Deines, P. The carbon isotopic composition of diamonds: relationship to diamond shape, color, occurrence and vapor composition. *Geochim. Cosmochim. Acta* **44**, 943–961 (1980).
43. Navon, O. Diamond formation in the Earth's mantle. In VII International Kimberlite Conference (eds J. J. Gurney, J. L. Gurney, M. D. Pascoe and S. H. Richadson). Red roof design, Cape Town, pp. 584–604 (1999).
44. Pal'yanov, Y. N., Sokol, A. G., Borzdov, Y. M., Khokhryakov, A. F. & Sobolev, N. V. Diamond formation from mantle carbonate fluids. *Nature* **400**, 417–418 (1999).
45. Cartigny, P. Stable isotopes and the origin of diamond. *Elements* **1**, 79–84 (2005).
46. Malkovets, V. G., Griffin, W. L., O'Reilly, S. Y. & Wood, B. J. Diamond, subcalcic garnet, and mantle metasomatism: Kimberlite sampling patterns define the link. *Geology* **35**, 339–342 (2007).
47. Stachel, T. & Harris, J. W. Syngenetic inclusions in diamond from the Birim field (Ghana)–a deep peridotitic profile with a history of depletion and re-enrichment. *Contrib. Mineral. Petrol.* **127**, 336–352 (1997).
48. Thomassot, E., Cartigny, P., Harris, J. W. & Viljoen (Fanus), K. S. Methane-related diamond crystallization in the Earth's mantle: stable isotope evidences from a single diamond-bearing xenolith. *Earth Planet. Sci. Lett.* **257**, 362–371 (2007).
49. Yamaoka, S., Akaishi, M., Kanda, H. & Osawa, T. Crystal growth of diamond in the system of carbon and water under very high pressure and temperature. *J. Cryst. Growth.* **125**, 375–377 (1992).
50. Akaishi, M. & Yamaoka, S. Crystallization of diamond from C-O-H fluids under high-pressure and high-temperature conditions. *J. Cryst. Growth.* **213**, 999–1003 (2000).
51. Palyanov, Y. N. & Sokol, A. G. The effect of composition of mantle fluids/melts on diamond formation processes. *Lithos* **112**, 690–700 (2009).
52. Sokol, A. G., Pal'yanov, Y. N., Pal'yanova, G. A., Khokhryakov, A. F. & Borzdov, Y. M. Diamond and graphite crystallization from C–O–H fluids. *Diam. Relat. Mater.* **10**, 2131–2136 (2001).
53. Sokol, A. G. & Pal'yanov, Y. N. Diamond formation in the system $MgO–SiO_2–H_2O–C$ at 7.5 GPa and 1,600 C. *Contrib. Mineral. Petrol.* **155**, 33–43 (2008).
54. Palyanov, Y. N., Shatsky, V. S., Sokol, A. G. & Sobolev, N. V. The role of mantle ultrapotassic fluids in diamond formation. *Proceedings of the National Academy of Sciences* **104**, 9122–9127 (2007).
55. Jablon, B. M. & Navon, O. Most diamonds were created equal. *Earth Planet. Sci. Lett.* **443**, 41–47 (2016).
56. Rohrbach, A. & Schmidt, M. W. Redox freezing and melting in the Earth's deep mantle resulting from carbon-iron redox coupling. *Nature* **472**, 209–212 (2011).

## Acknowledgements

We wish to thank Yury Borzdov and Alexander Khokhryakov for assistance throughout the study. The manuscript profited much from the thoughtful review by an anonymous reviewer. The research was performed by a grant of the Russian Science Foundation: grant 16-17-10041.

## Author Contributions

A.G.S. performed high-pressure experiments and made data analysis. T.A.B. and A.A.T. collected and interpreted GC/MS data. G.A.P. performed the thermodynamic calculations. A.G.S., A.A.T. and I.A.S. synthesised all collected data. A.G.S., A.A.T., T.A.B., I.A.S. and Yu.N.P. participated in the discussion and wrote the paper.

## Additional Information

**Supplementary information** accompanies this paper at doi:10.1038/s41598-017-00679-7

**Competing Interests:** The authors declare that they have no competing interests.

**Publisher's note:** Springer Nature remains neutral with regard to jurisdictional claims in published maps and institutional affiliations.